

# Optical Spectra of Candidate International Celestial Reference Frame (ICRF) Flat-Spectrum Radio Sources

O. Titov

Geoscience Australia, PO Box 378, Canberra, ACT 2601, Australia

[oleg.titov@ga.gov.au](mailto:oleg.titov@ga.gov.au)

Laura M. Stanford

Geoscience Australia, PO Box 378, Canberra, ACT 2601, Australia

Helen M. Johnston

Sydney Institute for Astronomy, School of Physics, University of Sydney, NSW 2006,  
Australia

T. Pursimo

Nordic Optical Telescope, Nordic Optical Telescope Apartado 474E-38700 Santa Cruz de  
La Palma, Santa Cruz de Tenerife, Spain

Richard W. Hunstead

Sydney Institute for Astronomy, School of Physics, University of Sydney, NSW 2006,  
Australia

David L. Jauncey

CSIRO Astronomy and Space Science, ATNF & Research School of Astronomy &  
Astrophysics, Australian National University, Canberra, ACT 2611, Australia

K. Maslennikov

The Central Astronomical Observatory at Pulkovo, Pulkovskoye Shosse, 65/1, 196140,  
St.Petersburg, Russia

– 2 –

and

A. Boldycheva

Ioffe Physical Technical Institute, 26 Polytekhnicheskaya, St. Petersburg, 194021, Russia

Received \_\_\_\_\_; accepted \_\_\_\_\_

## ABSTRACT

Continuing our program of spectroscopic observations of ICRF sources, we present redshifts for 120 quasars and radio galaxies. Data were obtained with five telescopes: the 3.58 m ESO New Technology Telescope (NTT), the two 8.2 m Gemini telescopes, the 2.5 m Nordic Optical Telescope (NOT), and the 6.0 m Big Azimuthal Telescope (BTA) of the Special Astrophysical Observatory in Russia.

The targets were selected from the International VLBI Service for Geodesy & Astrometry (IVS) candidate International Celestial Reference Catalogue which forms part of an observational VLBI program to strengthen the celestial reference frame. We obtained spectra of the potential optical counterparts of more than 150 compact flat-spectrum radio sources, and measured redshifts of 120 emission-line objects, together with 19 BL Lac objects. These identifications add significantly to the precise radio–optical frame tie to be undertaken by *Gaia*, due to be launched in 2013, and to the existing data available for analysing source proper motions over the celestial sphere. We show that the distribution of redshifts for ICRF sources is consistent with the much larger sample drawn from FIRST and SDSS, implying that the ultra-compact VLBI sources are not distinguished from the overall radio-loud quasar population.

In addition, we obtained NOT spectra for five radio sources from the FIRST and NVSS catalogs, selected on the basis of their red colors, which yielded three quasars with  $z > 4$ .

*Subject headings:* reference systems – galaxies: active – quasars: emission lines – BL Lacertae objects: general – radio continuum: general

## 1. Introduction

The coming astrometric space mission, *Gaia* (Perryman et al. 2001; Mignard & Klioner 2012), to be launched in 2013 by the European Space Agency, will measure high precision positions ( $\sim 26\mu\text{as}$  for  $V = 15$  mag,  $\sim 300\mu\text{as}$  for  $V = 20$  mag, (de Bruijne, 2012)) and proper motions of  $\sim 500,000$  quasars brighter than  $m_v = 20$ . This new optical astrometric catalog will be linked with the current radio astrometric catalog, ICRF2, the second realization of the International Celestial Reference Frame (Fey et al. 2009). Optical counterparts of the extragalactic sources are being sought to confirm their identification as quasars.

This paper is the second in our series aimed at investigating the optical spectra of radio sources in the International VLBI Service for Geodesy & Astrometry (IVS) Reference Catalog; see Schlüter & Behrend (2007) for a description of the IVS history. Astrometric Very Long Baseline Interferometry (VLBI) measures the differences in arrival times of radio waves from ultra-compact, flat-spectrum radio sources at telescopes positioned large distances apart. This procedure determines the positions of such sources to milliarcsecond precision.

The International Celestial Reference System (ICRS) (Arias et al. 1995) was adopted by the International Astronomical Union (IAU) as a reference system with its origin at the barycentre of the Solar system (MacCarthy & Petit 2004), and axes fixed by the positions of selected extragalactic radio sources. The first realization of the International Celestial Reference Frame (ICRF1) was used to establish the orientation of the ICRS axes (Ma et al. 1998). The current International Celestial Reference Frame, known as ICRF2, is based on a catalog of 295 ‘defining’ sources. The formal weighted errors in the radio positions are reported by Fey et al. (2009) to have an upper limit to the noise floor of  $41\mu\text{as}$ .

The IVS astrometric program has a total catalog of  $> 6000$  radio sources, where  $\sim 1200$

are observed on a regular basis. In the Southern Hemisphere, there is a significant deficit in candidate sources as well as a lack of optical identifications. By 2012 February, of the 3257 objects with measured redshifts only 1213 are in the southern hemisphere and only 287 have declinations south of  $-40^\circ$ . This paucity of redshifts in the south leads to problems in the analysis of apparent proper motions of the reference radio sources (Titov & Malkin 2009). To address this issue, an extensive program was started in 2010 to find optical counterparts and determine redshifts for southern IVS sources (Titov et al. 2011).

The quasars at high redshift ( $z \geq 2$ ) will be used for more intensive observations at the VLBI facilities in the southern hemisphere. VLBI observations of weak sources will be undertaken with the 64-meter telescope in Parkes, Australia, and two 26-meter telescopes in Hobart (Australia) and HartRAO (South Africa). Stronger radio sources (flux density  $\geq 400$  mJy) will be monitored with four 12-meter telescopes recently installed in Australia: the AuScope network comprising Hobart, Yarragadee and Katherine in Australia (Titov et al. 2013) and Warkworth in New Zealand. Several quasars found during the first observing run with the NTT in 2010 August (Titov et al. 2011) have now been tracked with the AuScope radio telescopes in 2011–2012.

In this paper we continue our spectroscopic observations of the optical counterparts of southern IVS sources, in particular those with a long VLBI observational history. Some strong radio sources from the northern hemisphere have also been observed. Optical identifications were sought initially from the image and catalog data from the SuperCOSMOS Sky Surveys on the grounds of their small digitization pixel scale and excellent astrometric accuracy (Hambly et al. 2001). We also took advantage of the Sloan Digital Sky Survey (SDSS; York et al. 2000) DR8 data release in the regions where it was available. This improved the identification process, especially in regions of high stellar density.

In addition, we observed five weaker radio sources from the NVSS (NRAO VLA Sky Survey; Condon et al. 1998) and FIRST catalogs (Faint Images of the Radio Sky at Twenty cm; Becker et al. 1995) that we identified with objects from the SDSS whose colors were typical of high redshift quasars. Such high redshift quasars provide unique information about the early stages of the Universe. The number of known radio sources with  $z \geq 4$  is small, and we are exploiting this technique in an attempt to increase their number.

The observations and data reduction procedures are described in Section 2 and we report our results, along with detailed comments on individual objects, in Section 3.

## 2. Observations

Spectroscopic observations were carried out at five optical facilities.

**ESO NTT:** We had a 5-night observing run in Visitor Mode at the European Southern Observatory (ESO) 3.58-meter New Technology Telescope at La Silla in 2011 December (088.A-0021 (A)) using the ESO Faint Object Spectrograph and Camera (EFOSC) system with grism #13 covering the wavelength range 3685–9315 Å. The seeing during observations was typically  $0''.5 - 1''.5$ , with a wavelength resolution 21.2 Å. Exposure times varied from 10 minutes to 1 hour depending on the magnitude of each target and current sky conditions. Wavelength calibration was performed using the spectra of a HeNeAr comparison lamp, resulting in an rms accuracy of 0.5 Å.

**Gemini:** A large number of targets were observed in Service Mode at the Gemini North and Gemini South 8.2-meter telescopes through the Poor Weather Program (GS-2011A-Q-89, GN-2011B-Q-109, GS-2011A-Q-94) using the Gemini Multi-Object Spectrograph (GMOS) system with grating R400. This grating covers 4500 Å centered either at 5200 Å or 6500 Å. As expected, the seeing and weather conditions were variable but the program overall was

very successful. The wavelength resolution was  $\sim 15 \text{ \AA}$ , and an exposure time of 20 minutes was used for all targets. Wavelength calibration was performed using the spectra of a CuAr lamp, resulting in an rms accuracy of  $\sim 0.3 \text{ \AA}$ .

**NOT:** Observations with the 2.5-meter Nordic Optical Telescope on La Palma were carried out using the Andalucia Faint Object Spectrograph and Camera (ALFOSC) spectrograph, either with grism #5, or grism #4 with the WG345 blocking filter. The nominal wavelength range for grism #4 is 3200–9100  $\text{\AA}$ , with the second-order blocking filter cutting below 3560  $\text{\AA}$ . The red end of the detector suffers fringing, so the effective long-wavelength limit is about 8000  $\text{\AA}$ . For grism #5 the nominal range is 5000–10250  $\text{\AA}$ . The slit width was  $1''.0$  or  $1''.3$  depending on the seeing. The typical integration time was between 20 and 40 minutes. The longer integrations were divided into two and the target was offset along the slit in order to improve the fringe correction. For the single integrations, internal halogen lamp images were taken before and after the science frame. Wavelength calibration was based on a HeNe lamp exposure taken before the science frame(s), resulting in an rms accuracy of  $\sim 0.5 \text{ \AA}$ .

**BTA:** Two objects were observed in Visitor Mode at the 6-meter Big Azimuthal Telescope (BTA) telescope, of the Special Astrophysical Observatory in Russia in 2011 August, using the SCORPIO multi-mode focal reducer with GR300 grism covering the wavelength range 3500–9500  $\text{\AA}$ . The seeing during observations was about  $2''$ . Spectral resolution was typically 20  $\text{\AA}$ .

Data reduction was performed with the IRAF software suite<sup>1</sup> using standard procedures for spectral analysis. We removed the bias and pixel-to-pixel gain variations from each

---

<sup>1</sup>IRAF is distributed by the National Optical Astronomical Observatories, which are operated by the Association of Universities for Research in Astronomy, Inc., under contract

frame and then removed cosmic rays using the IRAF task SZAP. Where more than one exposure was obtained, the separate exposures were combined. Spectrum extraction, sky subtraction and wavelength calibration were then carried out and the final one-dimensional spectra were flux-calibrated with a spectrophotometric standard observed with the same instrumental setup. Because the conditions were often non-photometric, especially for observations made through the Gemini Poor Weather Program, the flux calibration should be taken as approximate.

### 3. Results

Spectra of 120 IVS objects are shown in Fig. 1, along with the line identifications. A blue, dashed line indicates lines that were used for redshift calculation, while a red, dot-dashed line indicates lines that were detected, generally at a low signal-to-noise ratio (S/N), but not used in determining the mean redshift.

Table 1 lists the IVS sources with their ICRF2 coordinates (which refer to the epoch J2000.0), the telescope used for each spectrum, the identified emission lines with their rest and observed wavelengths, the mean redshift and error, and brief notes on individual sources. More detailed notes on individual sources (indicated by an asterisk in the final column) are given in section 3.2.

The quoted errors  $\Delta z$  in the mean redshift  $\bar{z}$  are given by

$$\Delta z = \{[(\sigma_z)^2 + (\Delta\lambda/\bar{\lambda}_0)^2]/N\}^{1/2},$$

where  $\sigma_z$  is the measured standard deviation among the independent estimates of  $z$ ,  $\Delta\lambda$  is the rms error in the wavelength calibration (typically 0.5 Å), and  $\bar{\lambda}_0$  is the mean

---

to the National Science Foundation.



rest wavelength of the  $N$  lines used to measure  $\bar{z}$ . Single-line redshifts (mostly Mg II) are assigned a conservative error of 0.001 if the signal-to-noise ratio is high and the line is symmetric. If the signal-to-noise ratio is low or the line is broad or asymmetric an (arbitrary) error of 0.002 has been assigned; in two extreme cases where the signal-to-noise ratio is low *and* the line is broad or asymmetric (IVS B0633–26B and B1129–161) the redshift is given with a colon(:) appended and no error.

Nineteen objects, listed in Table 2 with their ICRF2 positions (Fey et al. 2009), were found to have a good signal-to-noise ratio (typically  $S/N \sim 60 - 110$ ) but featureless spectra and hence are identified as probable BL Lac objects. Their spectra are shown in Fig. 2.

A further 18 targets had spectra with a signal-to-noise ratio that was too low for confident spectral classification; these are listed in Table 3 with their ICRF2 positions.

There were five IVS targets that returned stellar spectra. This was assumed to be the result of foreground obscuration and, in most cases, small but significant offsets between SuperCOSMOS optical and ICRF2 radio positions. In two cases the correct identification was found when the fields were reobserved in excellent seeing. Further discussion of these five objects is given in Section 3.1.

### 3.1. Separation of close objects

Occasionally, Galactic stars are found close on the sky to the radio position, leading to possible misidentification. Here we note several cases that were encountered during the observing runs.

- IVS B0900–664—the spectrum obtained was that of a red M star, which is offset by  $0''.52$  from the ICRF position. A faint counterpart was seen in the NTT B-band acquisition image, but a much longer integration in good seeing will be needed to

secure a redshift.

- IVS B0905–202—the nearest object, as seen by SuperCOSMOS, was a  $R = 14.6^m$  stellar object located  $1''.55$  from the radio position. Our NTT acquisition image, taken in  $0''.6$  seeing, showed a faint object at the radio position, but on the limb of the stellar disk. Spectroscopy of this faint  $R \sim 22$  object did not reveal any clear emission lines.
- IVS B1657–261—located in a very crowded star field in the Galactic bulge at a latitude of  $b = 9.7$ . Identification of the optical counterpart may not be feasible.
- IVS B1946–582—based on the SuperCOSMOS optical position, the radio minus optical position difference is only  $0''.06$  in right ascension and  $-0''.04$  in declination, but the Gemini South observation of this  $R \sim 19$  object showed a typical stellar spectrum. The radio source has a flat spectrum with flux density 200–300 mJy at cm wavelengths.
- IVS B2300–307—the obscuration of the optical field of this source by a foreground star was discussed previously (Titov et al. 2011). However, a later 80 s image in  $0''.6$  seeing (Fig. 3) revealed a faint  $R \sim 22$  object coincident with the radio position. Our spectroscopy yielded a redshift of  $1.039 \pm 0.002$  based on weak C III] and Mg II emission.

### 3.2. Notes on individual targets

- IVS B0233–478—the broad feature attributed to Al III and C III] may also include Si III  $\lambda 1890$ .
- IVS B0417–302—prominent Fe II multiplet emission; intervening Mg II doublet absorption at  $z_{\text{abs}} = 0.8395 \pm 0.0005$ .

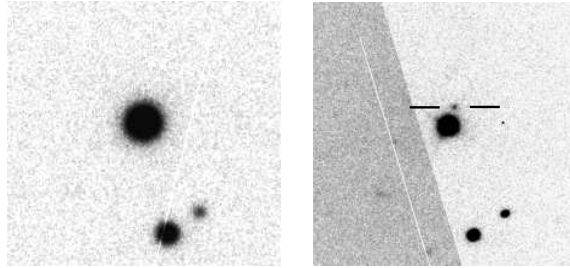


Fig. 3.— Two acquisition images of the sky field around the quasar IVS B2300–307 made at the NTT in 2010 August (left: seeing  $2''$ ) and 2011 December (right: seeing  $0''.6$ ). Each image is  $50''$  on a side; north is up and east to the left. The foreground star in the centre of the left image completely obscures the quasar due to its large seeing disk. In the right image the much better seeing reveals the faint quasar ( $R \sim 22$ , marked between the bars), separated by  $3''.7$  from the star. (The diagonal step in contrast in the right image is an artefact of fast readout using two amplifiers for the acquisition image.)

- IVS B0447–507—possible double-peaked C III] line and prominent Fe II multiplet bands.
- IVS B0448–482—poor redshift match to C III] may indicate the presence of Si III  $\lambda 1890$ ; prominent Fe II multiplet bands.
- IVS B0521–262—strong associated absorption in the Ly  $\alpha$  emission line and a clear detection of the Lyman limit at the emission redshift.
- IVS B0529–031—faint optical counterpart with a very red spectrum, showing a single broad emission line identified as Mg II with associated Mg II absorption at  $z_{\text{abs}} = 1.8744 \pm 0.0004$ , corresponding to a relative blue-shift of  $\sim 1500 \text{ km s}^{-1}$ ; a further absorption line, at  $8182.1 \text{ \AA}$  remains unidentified. Given the low signal blueward of  $6000 \text{ \AA}$ , together with the faint SDSS blue magnitudes ( $u = 24.41$ ,  $g = 21.93$ ), it is not surprising that C III] and C IV are not detected.

- IVS B0548–527—redshift in Table 1 is for the forbidden lines; the permitted lines of Mg II and H  $\beta$  show a redshift systematically higher by  $830 \pm 80 \text{ km s}^{-1}$ .
- IVS B0554+242—narrow self-absorption in Ly  $\alpha$  and C IV at  $z_{\text{abs}} = 3.2319 \pm 0.0010$ .
- IVS B0608–230—wavelengths for C III] and C IV are not consistent, suggesting the presence of additional lines or asymmetric structure; in addition, the Ly  $\alpha$  wavelength is likely to be affected by absorption in the blue wing.
- IVS B0633–26B—a very faint galaxy; a low signal-to-noise ratio spectrum, with a single broad emission line, assumed to be Mg II.
- IVS B0810–180—very broad line wings in C IV and Ly  $\alpha$ , extending  $\sim 30,000 \text{ km s}^{-1}$  redward of the line peaks.
- IVS B0828–064—poor consistency in redshift between C IV and C III], possibly due to associated absorption in the blue wing of C IV. Mg II is present with a low signal-to-noise ratio just redward of the atmospheric A-band.
- IVS B0844–557—redshift in Table 1 is for the forbidden lines; permitted lines Mg II and H  $\beta$  are displaced  $\sim 1000 \text{ km s}^{-1}$  to higher redshift.
- IVS B0948–860—single emission line, assumed to be Ly  $\alpha$ ; the adopted redshift,  $z = 3.696$ , is consistent with the 40% continuum depression blueward of the emission line due to the Ly  $\alpha$  forest, and the possible detection of C IV at the red edge of the spectrum.
- IVS B0952–185—associated absorption at the emission redshift in both Ly  $\alpha$  and C IV.
- IVS B0956–409—Ly  $\alpha$  is strongly self-absorbed.

- IVS B1004–125—reported as having  $z = 0.24$  in Simbad (no reference given), clearly inconsistent with our Gemini spectrum; strong intervening heavy-element system at  $z_{\text{abs}} = 1.5786 \pm 0.0002$  based on Fe II  $\lambda\lambda 2344, 2382, 2586, 2600$  and Mg II  $\lambda\lambda 2796, 2803$  absorption.
- IVS B1020+270—extended red wing in C IV; C III] is not detected due to strong CCD fringing.
- IVS B1039–474—Si IV, C IV and C III] emission lines all show strongly extended blue wings; redshift is based on the peak positions of the lines.
- IVS B1127–443—single-line redshift is supported by stellar absorption features (G-band, Mg Ib) noted in the plotted spectrum.
- IVS B1143–696—spectrum is very similar to that of 3C 273, with strong Fe II multiplet emission in the region around H  $\beta$  (Wampler & Oke 1967).
- IVS B1722+562—strong associated absorption system at  $z_{\text{abs}} = 2.2463 \pm 0.0002$  seen in C IV, Si IV, N V and Ly  $\alpha$ . This has led to a relatively large uncertainty in emission redshift.
- IVS B2235–556—strong self-absorption in the red wing of C IV.
- IVS B2334–525—broad Mg II, possibly double-peaked with an extended red wing.
- IVS B2341+295—very blue object based on POSS II sky survey images; rise in the spectrum redward of  $7000 \text{ \AA}$  may be due to the underlying galaxy or an unrelated object on the spectrograph slit. Intervening Mg II absorber at  $z = 0.8644 \pm 0.0004$ .

### 3.3. Spectra of color-selected quasars

In an attempt to find more high-redshift radio quasars for our VLBI proper motion studies as a function of redshift, we selected five weak radio sources from the FIRST and NVSS catalogs for which the SDSS colors suggested the likelihood of  $u$ - or  $g$ -band dropouts and the possibility of high redshifts. Spectra were obtained at the NOT on the nights of 2012 May 24–26. The SDSS colors, wavelengths and redshifts for the five color-selected radio quasars are given in Table 4. The ‘bluest’ of the five, NVSS J125944+240707, was a  $z = 1.139$  radio galaxy, but the other four proved to be broad emission-line quasars with redshifts in excess of 3.5, including three with  $z > 4$ . This is an excellent return for our search and a striking result from the NOT, the smallest of the telescopes used in this program. The five spectra are shown in Fig. 4 and further information is given in Table 4. Redshifts for the  $z > 4$  quasars are based on estimated wavelengths for  $\text{Ly}\alpha$  (and, in one case,  $\text{Ly}\beta$ ) and are very uncertain because of strong absorption in the blue wing of the line.

A comparison between the FIRST and NVSS flux densities at 1.4 GHz for the five sources showed that one, NVSS J145459+110928, appeared to show evidence of variability, with  $S_{\text{NVSS}} = 9.8 \pm 0.5$  mJy and  $S_{\text{FIRST}} = 15.07 \pm 0.14$  mJy. This is also the only source that is unresolved in FIRST. The other four sources all show minor extension at the  $1''$  level.

## 4. Redshift distributions

Together with the 31 redshifts reported in Titov et al. (2011), we have now accumulated over 150 redshifts for IVS sources, mostly in the south. Their optical counterparts are systematically fainter than those in the Titov & Malkin (2009) compilation. Since the IVS selection process is directed at compact, milliarcsecond radio quasars, it is important to

test whether their redshift distribution differs from that of the FIRST-SDSS quasar sample (Kimball et al. 2011), which is selected without regard to morphology, spectral index or angular size and extends to much lower flux densities.

The redshift distribution of the sources from this paper and Titov et al. (2011) is shown in Figure 5(a). For comparison, Figure 5(b) shows the distribution of 1594 point sources with known redshifts from ICRF2, using redshift data from Titov & Malkin (2009). The SuperCOSMOS Hambly et al. (2001) morphological classification was used to remove galaxies from the Titov & Malkin (2009) list, and the sample was further restricted to those with radio-optical offsets  $< 1''$  and Galactic latitudes  $> 10^\circ$  (Schaefer et al. 2013, in prep.).

The redshift distribution for the sources from this paper and the earlier paper (Titov et al. 2011) is completely consistent with having been drawn from the same redshift distribution as FIRST-SDSS quasars (Kimball et al. 2011), with a Kolmogorov-Smirnov test giving a probability  $p = 0.84$  of the two samples being drawn from the same distribution. Thus the sharp drop-off that we see in the number of quasars at  $z \gtrsim 2$  is a reflection of the underlying quasar distribution, and not a selection effect of the IVS candidate sources. While the K-S plot for the ICRF2 sample shows an apparent excess of low-redshift sources compared with FIRST-SDSS, the difference is not significant, with a K-S probability of  $p = 0.24$ . We attribute this excess to selection effects arising from the redshifts in (Titov & Malkin 2009) being drawn from the literature, and therefore likely to be biased towards brighter, lower-redshift quasars.

## 5. Summary and conclusion

We present redshifts and spectra for 120 emission-line objects identified with radio sources from the candidate International Celestial Reference Catalog. Most of the target

objects are in the south and many had not previously been optically identified. While redshifts were usually based on two or more lines, those for 22 objects were based on a single emission line, in most cases assumed to be Mg II; many of these single-line redshifts were supported by other spectral information and most are considered reliable. In addition, we classed 19 sources as probable BL Lac objects, based on a high signal-to-noise ratio but featureless spectra. A further 18 targets were considered to have a signal-to-noise ratio too low for confident spectral classification.

The distribution of redshifts from this paper, together with those from our earlier paper (Titov et al. 2011), is consistent with the much larger sample drawn from FIRST and SDSS (Kimball et al. 2011). This implies that the ultra-compact, flat-spectrum sources that make up the IVS Reference Catalog are not distinguished from the radio quasar population at large. On the other hand, the distribution of redshifts from the much larger sample drawn from ICRF2 (Titov & Malkin 2009) has a small, but not significant excess of low-redshift quasars, almost certainly the result of observational selection.

## 6. Acknowledgments

This paper is based on observations collected at five telescopes:

1. ESO New Technology Telescope, under the European Organisation for Astronomical Research in the Southern Hemisphere, Chile under program 088.A-0021(A).
2. Two Gemini Observatories, which are operated by the Association of Universities for Research in Astronomy, Inc., under a cooperative agreement with the National Science Foundation on behalf of the Gemini partnership: the National Science Foundation (United States), the Science and Technology Facilities Council (United Kingdom), the National Research Council (Canada), CONICYT (Chile), the Australian Research Council



(Australia), Ministerio da Ciuncia, Tecnologia e Inovacio (Brazil) and Ministerio de Ciencia, Tecnologia e Innovacion Productiva (Argentina) under programs GS-2011A-Q-89 and GS-2011B-Q-94 (Gemini South), and GN-2011B-Q-109 (Gemini North).

3. Six-meter Big Azimuthal Telescope (BTA) operated by the Special Astrophysical Observatory (Russia)

4. Nordic Optical Telescope, operated on the island of La Palma jointly by Denmark, Finland, Iceland, Norway and Sweden, in the Spanish Observatorio del Roque de los Muchachos of the Instituto de Astrofisica de Canarias.

Two of us, Titov and Jauncey, were supported by a travel grant from the Australian Nuclear Science Technology Organisation (ANSTO) in their Access to Major Research Facilities Program (AMRFP) (reference number AMRFP 10/11-O-31) to travel to the BTA telescope in Russia.

Funding for SDSS-III has been provided by the Alfred P. Sloan Foundation, the Participating Institutions, the National Science Foundation and the U.S. Department of Energy Office of Science. The SDSS-III web site is <http://www.sdss3.org/>.

SDSS-III is managed by the Astrophysical Research Consortium for the Participating Institutions of the SDSS-III Collaboration including the University of Arizona, the Brazilian Participation Group, Brookhaven National Laboratory, University of Cambridge, Carnegie Mellon University, University of Florida, the French Participation Group, the German Participation Group, Harvard University, the Instituto de Astrofisica de Canarias, the Michigan State/Notre Dame/JINA Participation Group, Johns Hopkins University, Lawrence Berkeley National Laboratory, Max Planck Institute for Astrophysics, Max Planck Institute for Extraterrestrial Physics, New Mexico State University, New York University, Ohio State University, Pennsylvania State University, University of Portsmouth,

Princeton University, the Spanish Participation Group, University of Tokyo, University of Utah, Vanderbilt University, University of Virginia, University of Washington, and Yale University.

AuScope is funded under the National Collaborative Research Infrastructure Strategy (NCRIS), an Australian Commonwealth Government Programme.

This paper is published with the permission of the CEO, Geoscience Australia.

© Commonwealth of Australia (Geoscience Australia) 2013. This product is released under the Creative Commons Attribution 3.0 Australia Licence.  
<http://creativecommons.org/licenses/by/3.0/au/deed.en>

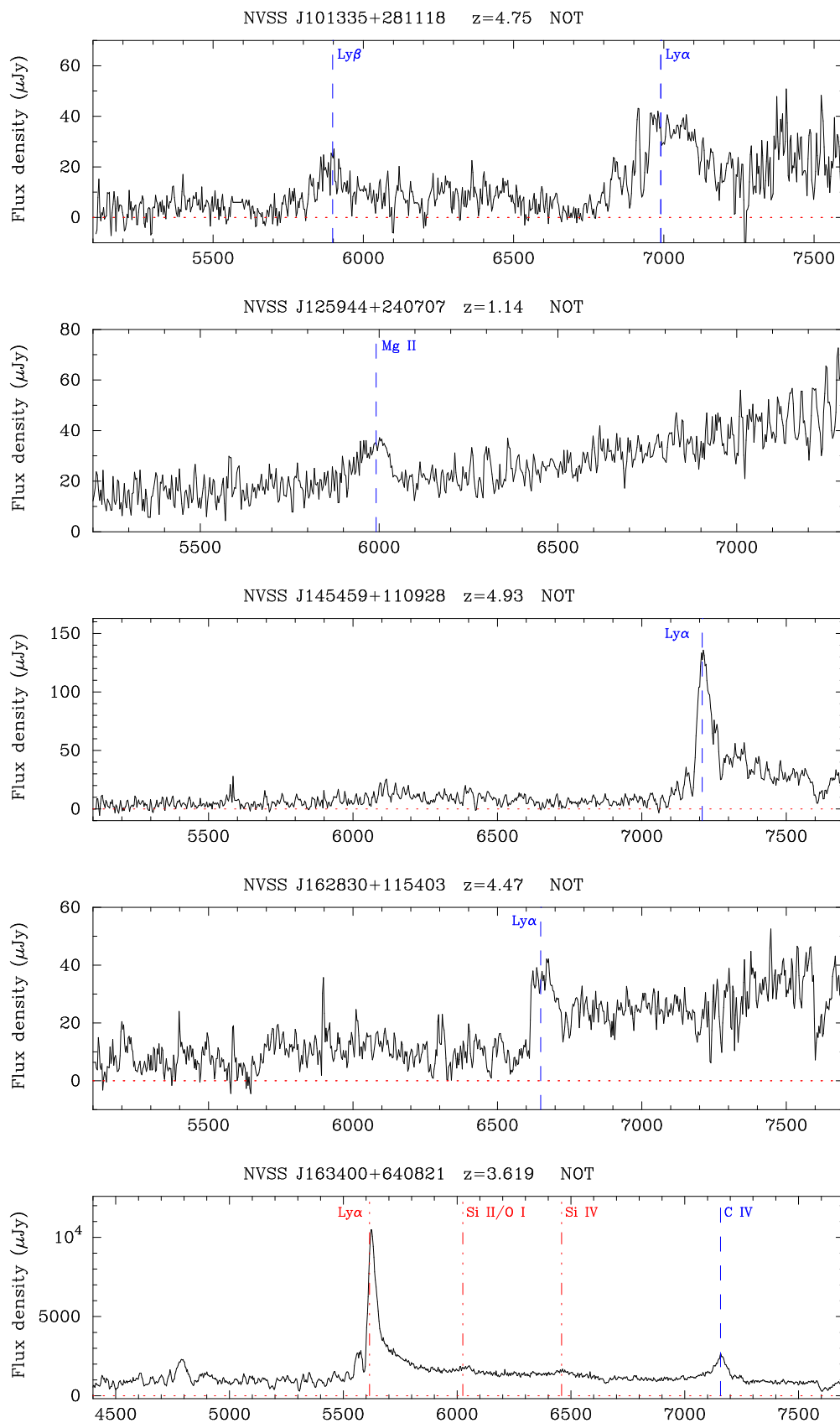


Fig. 4.— Spectra of the five color-selected quasars from NVSS/FIRST and SDSS. Dashed lines (blue) indicate emission lines used for redshift determination; dot-dashed lines (red)

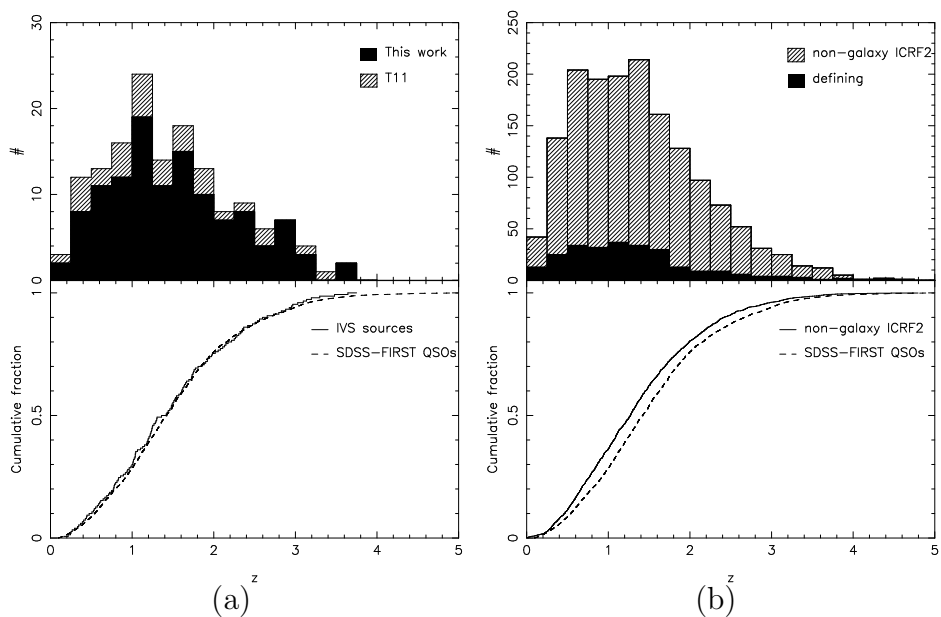


Fig. 5.— (a) Distribution of redshifts among the  $\sim 150$  IVS sources from this paper and the previous paper (Titov et al. 2011, abbreviated above as T11). The lower panel shows the cumulative redshift distribution (K-S test) compared with the FIRST-SDSS sample (Kimball et al. 2011). (b) Corresponding redshift distribution and K-S test for 1594 ICRF2 quasars from Titov & Malkin (2009); see text.

## REFERENCES

- Afanas'ev, V. L., Dodonov, S. N., Moiseev, A. V., et al. 2009, *ARep*, 53, 287
- Arias, E. F., Charlot P., Feissel, M., & Lestrade, J.-F. 1995, *A&A*, 303, 604
- Becker, R. H., White, R. L., & Helfand, D. J., 1995, *ApJ*, 450, 559
- Condon, J. J., Cotton, W. D., Greisen, E. W., et al. 1998, *AJ*, 115, 1693
- de Bruijne, J. H. J., 2012, *Ap&SS*, Vol 341, Issue 1, 31
- Fey, A., Gordon, G., & Jacobs, C. (eds.), 2009, *The Second realization of the International Celestial Reference Frame by Very Long Baseline Interferometry*, IERS Technical Notes 35, Verlag des Bundesamts für Kartographie und Geodäsie, Frankfurt am Main
- Hambly, N. C., Davenhall, A. C., Irwin, M. J., & MacGillivray, H. T., 2001, *MNRAS*, 326, 1315
- Jones, D. H., Read, M. A., Saunders, W., et al. 2009, *MNRAS*, 399,683
- Kimball, A. E., Ivezić, Z., Wiita, P. J., & Schneider, D. P., 2011, *AJ*, 141, 182
- Ma, C., Arias, E. F., & Eubanks, T. M., 1998, *AJ*, 116, 516
- MacCarthy, D. & Petit G. (eds.), 2004, *IERS Conventions (2003)*, IERS Technical Notes 32, Verlag des Bundesamts für Kartographie und Geodäsie, Frankfurt am Main
- Mignard, F. & Klioner, S., 2012, *A&A*, 547. A59
- Ojha, R., Fey, A. L., Charlot, P., et al. 2005, *AJ*, 130, 2529
- Perryman, M. A. C., de Boer, K. S., Gilmore, G., et al. 2001, *A&A*, 369, 339

Quiniento, Z. M. & Cersosimo, J. C. 1993, A&AS, 97, 435

Schlüter, W. & Behrend D. 2007, JG, 81, 379

Shaw, M. S., Romani, R. W., Cotter, G. H., et al. 2012, ApJ, 748, 49

Titov, O., & Malkin, Z. 2009, A&A, 506, 1477

Titov, O., Jauncey, D. L., Johnston, H. M., et al. 2011, AJ, 142, 165

Titov, O., Dickey, J. M., Lovell, J. E. J., & McCulloch, P. M., 2013, Proc. IAG Symp. 139

Wampler, E. J. & Oke, J. B. 1967, ApJ, 148, 695

York, D. G., Adelman, J., Anderson, J. E., Jnr, et al. 2000, AJ, 120, 1579

Table 1. Observed emission lines

Source	RA (J2000) <sup>a</sup>	Dec (J2000) <sup>a</sup>	Telescope <sup>b</sup>	Line	Rest $\lambda$	Obs $\lambda^c$	$\bar{z}$	Note <sup>d</sup>
IVS B0022–227	00 25 24.2474	–22 27 47.596	GS	Mg II	2799.9	5136.3	$0.834 \pm 0.001$	S
IVS B0032+276	00 34 43.4861	+27 54 25.721	BTA	Ly $\alpha$	1215.7	4820.4	$2.9642 \pm 0.0009$	
				N V	1240.1	[4921.7]		
				Si IV	1398.3	[5545.9]		
				C IV	1549.5	6141.2		
IVS B0044–846	00 44 26.6883	–84 22 39.988	GS	Mg II	2799.9	5697.2	$1.035 \pm 0.001$	S $z = 1.032$ [S12]
IVS B0205–619	02 06 40.0029	–61 43 32.206	NTT	C II]	2326.9	[4032.5]	$0.7316 \pm 0.0010$	
				Mg II	2799.9	4855.9		
				[O II]	3726.8	6454.0		
				[Ne III]	3868.7	6694.0		
				[O III]	5006.8	8661.5		
IVS B0206–625	02 08 01.1713	–62 16 35.533	GS/NTT	Ly $\alpha$	1215.7	4114.9	$2.3817 \pm 0.0016$	
				N V	1240.1	[4198.6]		
				Si IV	1398.3	[4733.6]		
				C IV	1549.5	5237.6		
				C III]	1908.7	6451.8		
IVS B0213–015	02 16 05.6638	–01 18 03.397	GS	Ly $\alpha$	1215.7	4624.9	$2.8028 \pm 0.0017$	
				N V	1240.1	[4720.2]		
				Si IV	1398.3	[5326.7]		
				C IV	1549.5	5887.3		
				C III]	1908.7	7261.7		
IVS B0219–637	02 20 54.1727	–63 30 19.387	GS	C III]	1908.7	4730.2	$1.4780 \pm 0.0003$	
				Mg II	2799.9	6937.4		
IVS B0226–375	02 28 33.7343	–37 19 56.338	NTT	Ly $\alpha$	1215.7	3842.4	$2.1538 \pm 0.0034$	
				Si IV	1398.3	[4408.5]		
				C IV	1549.5	4881.0		
				C III]	1908.7	6014.0		
IVS B0233–478	02 35 06.4235	–47 37 10.574	GS	Al III	1858.8	[4692.1]	$1.504 \pm 0.001$	S *
				C III]	1908.7	[4784.9]		
				Mg II	2799.9	7011.2		
IVS B0301–721	03 01 38.4456	–71 56 34.399	GS	Mg II	2799.9	5105.8		

Table 1—Continued

Source	RA (J2000) <sup>a</sup>	Dec (J2000) <sup>a</sup>	Telescope <sup>b</sup>	Line	Rest $\lambda$	Obs $\lambda^c$	$\bar{z}$	Note <sup>d</sup>
				[O II]	3726.8	6795.7		
				[Ne III]	3868.7	7051.2	$0.8232 \pm 0.0003$	
IVS B0318–388	03 20 46.4048	–38 37 28.503	NTT	C III]	1908.7	4191.0		
				Mg II	2799.9	6151.3	$1.1964 \pm 0.0006$	
IVS B0319–056	03 21 59.8703	–05 26 12.429	NTT	Mg II	2799.9	4417.8		
				H $\gamma$	4340.5	6843.3		
				H $\beta$	4861.3	7686.5	$0.5785 \pm 0.0014$	
IVS B0319–315	03 21 28.7402	–31 22 56.336	NTT	Si IV	1398.3	[3900.0]		
				C IV	1549.5	4316.8		
				C III]	1908.7	5312.2		
				Mg II	2799.9	[7783.9]	$1.7845 \pm 0.0014$	
IVS B0340–600	03 41 21.6148	–59 54 08.907	GS	C IV	1549.5	4746.4		
				He II	1640.4	5026.6		
				C III]	1908.7	5847.5	$2.0637 \pm 0.0004$	
IVS B0341+158	03 44 23.1721	+15 59 43.369	GS/NOT	Ly $\alpha$	1215.7	3993.3		
				C IV	1549.5	5071.8		
				C III]	1908.7	6240.7	$2.276 \pm 0.005$	
IVS B0343+485	03 47 11.6133	+48 42 37.473	GN	C III]	1908.7	[5798.6]		
				Mg II	2799.9	8519.1	$2.043 \pm 0.002$	S
IVS B0346+514	03 50 25.0515	+51 38 38.734	GN	Mg II	2799.9	6823.8	$1.437 \pm 0.001$	S
IVS B0355–669	03 55 47.8834	–66 45 33.817	GS	Mg II	2799.9	4970.3		
				[Ne V]	3425.5	6081.2		
				[O II]	3726.8	6619.3		
				[Ne III]	3868.7	6866.0		
				[Ne III]	3969.8	[7052.8]		
				H $\delta$	4101.7	[7285.6]	$0.7753 \pm 0.0003$	
IVS B0410–519	04 11 37.1499	–51 49 23.350	GS/NTT	C III]	1908.7	4306.7		
				Mg II	2799.9	6319.2	$1.2566 \pm 0.0003$	
IVS B0412–779	04 10 42.3092	–77 50 43.293	GS	Si IV	1398.3	[4820.2]		
				C IV	1549.5	5343.9		



Table 1—Continued

Source	RA (J2000) <sup>a</sup>	Dec (J2000) <sup>a</sup>	Telescope <sup>b</sup>	Line	Rest $\lambda$	Obs $\lambda^c$	$\bar{z}$	Note <sup>d</sup>
				He II	1640.4	[5656.4]		
				C III]	1908.7	6583.0	$2.4489 \pm 0.0002$	
IVS B0416–216	04 19 00.4182	–21 32 35.675	NTT	C IV	1549.5	4103.8		
				C III]	1908.7	5044.8		
				Mg II	2799.9	[7428.9]	$1.6458 \pm 0.0027$	
IVS B0417–302	04 19 47.2054	–30 10 23.835	GS	Mg II	2799.9	5609.2	$1.003 \pm 0.002$	S *
IVS B0418–151	04 20 18.3933	–15 01 26.576	NTT	C III]	1908.7	4160.1		
				Mg II	2799.9	6102.3	$1.1795 \pm 0.0002$	
IVS B0428–042	04 31 28.0885	–04 06 27.319	GS	Mg II	2799.9	4556.9		
				[O II]	3726.8	6065.9		
				[Ne III]	3868.7	6298.0		
				H $\gamma$	4340.5	[7072.0]		
				[O III]	4363.2	[7098.9]		
				H $\beta$	4861.3	[7918.0]		
				[O III]	4958.9	8072.2		
				[O III]	5006.8	8151.6	$0.6278 \pm 0.0002$	
IVS B0432–606	04 33 34.1084	–60 30 13.769	GS	Mg II	2799.9	5403.6		
				[Ne V]	3345.4	6458.1		
				[Ne V]	3425.5	6612.6		
				[O II]	3726.8	7193.1	$0.9301 \pm 0.0002$	
IVS B0432+254	04 35 34.5829	+25 32 59.696	GN	[Ne V]	3425.5	[5483.6]		
				H $\epsilon$	3969.8	[6364.5]		
				H $\delta$	4101.7	[6573.0]		
				H $\gamma$	4340.5	[6952.7]		
				H $\beta$	4861.3	7792.2		
				[O III]	4958.9	7942.9		
				[O III]	5006.8	8021.0	$0.6021 \pm 0.0003$	
IVS B0437–303	04 39 53.2015	–30 17 45.624	GS/NTT	C IV	1549.5	3793.0		
				He II	1640.4	[4016.3]		
				C III]	1908.7	4669.5		
				Mg II	2799.9	6851.0	$1.4466 \pm 0.0002$	
IVS B0446–265	04 48 23.9646	–26 26 14.821	NTT	Si IV	1398.3	[3862.7]		

Table 1—Continued

Source	RA (J2000) <sup>a</sup>	Dec (J2000) <sup>a</sup>	Telescope <sup>b</sup>	Line	Rest $\lambda$	Obs $\lambda^c$	$\bar{z}$	Note <sup>d</sup>
				C IV	1549.5	4282.5		
				C III]	1908.7	5276.4		
				Mg II	2799.9	[7731.9]	$1.7641 \pm 0.0004$	
IVS B0447–507	04 48 22.3029	–50 41 33.827	GS	C III]	1908.7	4724.1		
				Mg II	2799.9	6949.0	$1.4785 \pm 0.0034$	*
IVS B0448–482	04 49 39.5904	–48 09 40.709	GS	Al III	1858.8	[4683.2]		
				C III]	1908.7	[4765.2]		
				Mg II	2799.9	6992.4	$1.497 \pm 0.001$	S *
IVS B0450–469	04 51 53.3452	–46 53 19.888	GS	Mg II	2799.9	4485.8		
				[Ne V]	3425.5	5486.0		
				[O II]	3726.8	5970.9		
				[Ne III]	3868.7	6196.0		
				[Ne III]	3969.8	6355.7		
				H $\delta$	4101.7	[6562.1]		
				H $\gamma$	4340.5	6952.9		
				[O III]	4363.2	6986.5	$0.6016 \pm 0.0002$	
IVS B0455–183	04 57 54.3252	–18 19 16.072	GS	C III]	1908.7	4825.1		
				Mg II	2799.9	7071.2	$1.5267 \pm 0.0012$	
IVS B0503–608	05 04 01.7011	–60 49 52.539	NTT	Mg II	2799.9	5702.0	$1.037 \pm 0.002$	S
IVS B0511+009	05 13 40.0325	+01 00 21.654	NTT	Ly $\alpha$	1215.7	4479.2		
				N V	1240.1	[4566.9]		
				Si IV	1398.3	[5156.0]		
				C IV	1549.5	5698.4		
				C III]	1908.7	7016.5	$2.6794 \pm 0.0026$	
IVS B0514–156	05 16 57.1855	–15 37 10.367	NTT	C IV	1549.5	4029.7		
				C III]	1908.7	4948.2		
				Mg II	2799.9	7257.3	$1.5950 \pm 0.0028$	
IVS B0515–053	05 17 28.1101	–05 20 40.842	NTT	C IV	1549.5	[3744.3]		
				C III]	1908.7	4602.1		
				Mg II	2799.9	6760.8	$1.4129 \pm 0.0018$	
IVS B0519–176	05 21 23.5574	–17 37 30.184	GS	[O II]	3726.8	5022.4		

Table 1—Continued

Source	RA (J2000) <sup>a</sup>	Dec (J2000) <sup>a</sup>	Telescope <sup>b</sup>	Line	Rest $\lambda$	Obs $\lambda^c$	$\bar{z}$	Note <sup>d</sup>
				[Ne III]	3868.7	[5213.1]		
				H $\beta$	4861.3	6548.4		
				[O III]	4958.9	6686.0		
				[O III]	5006.8	6744.8	$0.3475 \pm 0.0003$	
IVS B0520–165	05 22 44.6549	–16 27 52.405	NTT	Si IV	1398.3	[4105.3]		
				C IV	1549.5	4532.1		
				C III]	1908.7	5588.8		
				Mg II	2799.9	[8220.0]	$1.9265 \pm 0.0016$	
IVS B0521–262	05 23 18.4695	–26 14 09.555	NTT	Ly $\alpha$	1215.7	[5020.9]		
				Si IV	1398.3	[5773.0]		
				C IV	1549.5	6366.5		
				C III]	1908.7	7842.3	$3.1087 \pm 0.0002$	*
IVS B0524–485	05 26 16.6713	–48 30 36.791	NTT	C III]	1908.7	4393.6		
				Mg II	2799.9	6457.5	$1.3041 \pm 0.0022$	$z = 1.299$ [S]
IVS B0529–031	05 32 07.5192	–03 07 07.037	GN	Mg II	2799.9	8063.7	$1.880 \pm 0.002$	S *
IVS B0548–527	05 49 43.8055	–52 46 25.962	NTT	Mg II	2799.9	4061.2		
				[Ne V]	3425.5	4956.9		
				[O II]	3726.8	5392.3		
				[Ne III]	3868.7	[5603.7]		
				[Ne III]	3967.8	[5743.2]		
				H $\delta$	4101.7	[5931.7]		
				H $\gamma$	4340.5	[6303.7]		
				[O III]	4363.2	[6314.3]		
				H $\beta$	4861.3	7053.1		
				[O III]	4958.9	7171.7		
				[O III]	5006.8	7242.2	$0.4467 \pm 0.0002$	*
IVS B0554+242	05 57 04.7135	+24 13 55.298	NOT	Ly $\alpha$	1215.7	5148.3		
				C IV	1549.5	6541.6	$3.228 \pm 0.007$	*
IVS B0558+234	06 01 47.3569	+23 24 53.484	GN	H $\beta$	4861.3	6205.1		
				[O III]	4958.9	6311.4		
				[O III]	5006.8	6373.6		
				He I	5875.6	[7494.5]		
				H $\alpha$	6562.8	8356.7		

Table 1—Continued

Source	RA (J2000) <sup>a</sup>	Dec (J2000) <sup>a</sup>	Telescope <sup>b</sup>	Line	Rest $\lambda$	Obs $\lambda^c$	$\bar{z}$	Note <sup>d</sup>
				[N II]	6583.5	8381.7	$0.2737 \pm 0.0007$	
IVS B0559–276	06 01 48.7208	–27 36 22.011	NTT	C IV	1549.5	4125.9		
				C III]	1908.7	5083.6		
				Mg II	2799.9	7461.8	$1.6637 \pm 0.0007$	
IVS B0559–200	06 01 52.8263	–20 04 45.212	NTT	C III]	1908.7	4244.2		
				Mg II	2799.9	6226.8	$1.2238 \pm 0.0002$	* $z = 1.216$ [S12]
IVS B0601+245	06 04 55.1213	+24 29 55.036	NOT	C III]	1908.7	[4068.2]		
				Mg II	2799.9	5972.3	$1.133 \pm 0.002$	S
IVS B0608–230	06 10 38.7873	–23 01 45.836	NTT	Ly $\beta$	1025.7	[3978.2]		
				Ly $\alpha$	1215.7	4688.8		
				N V	1240.1	[4766.8]		
				Si IV	1398.3	[5390.8]		
				C IV	1549.5	5957.8		
				C III]	1908.7	7367.8	$2.854 \pm 0.005$	*
IVS B0620–194	06 22 28.5370	–19 27 18.178	NTT	Ly $\alpha$	1215.7	[3900.0]		
				N V	1240.1	[3963.9]		
				Si IV	1398.3	[4481.8]		
				C IV	1549.5	4941.1		
				C III]	1908.7	6089.2	$2.1895 \pm 0.0007$	
IVS B0633–26B	06 35 19.4162	–26 20 55.717	NTT	Mg II	2799.9	7467.0	1.67 :	S *
IVS B0642–617	06 42 46.9991	–61 50 08.674	NTT	C III]	1908.7	4243.5		
				Mg II	2799.9	6224.4	$1.2232 \pm 0.0001$	
IVS B0657–586	06 58 13.7788	–58 40 27.567	NTT	Mg II	2799.9	[3985.7]		
				[O II]	3726.8	5299.9		
				[O III]	4958.9	7045.9		
				[O III]	5006.8	7114.8	$0.4213 \pm 0.0004$	
IVS B0718–622	07 19 04.4740	–62 18 02.444	NTT	C III]	1908.7	4288.3		
				Mg II	2799.9	6289.4		
				[O II]	3726.0	[8376.6]	$1.2465 \pm 0.0003$	
IVS B0726–132	07 29 17.8177	–13 20 02.271	NTT	H $\beta$	4861.3	[6512.0]		

Table 1—Continued

Source	RA (J2000) <sup>a</sup>	Dec (J2000) <sup>a</sup>	Telescope <sup>b</sup>	Line	Rest $\lambda$	Obs $\lambda^c$	$\bar{z}$	Note <sup>d</sup>
				[O III]	4958.9	6659.1		
				[O III]	5006.8	6729.8	$0.3435 \pm 0.0006$	
IVS B0728–320	07 30 38.2983	–32 08 20.176	NTT	Mg II	2799.9	4249.5		
				[O II]	3726.8	5652.6		
				H $\gamma$	4340.5	[6576.3]		
				[O III]	4363.2	6613.2		
				H $\beta$	4861.3	[7355.1]		
				[O III]	4958.9	7510.5		
				[O III]	5006.8	7584.2	$0.5159 \pm 0.0006$	
IVS B0748–006	07 51 10.2050	–00 46 51.055	NTT	Ly $\alpha$	1215.7	3779.5		
				Si IV	1398.3	[4342.6]		
				C IV	1549.5	4804.4		
				C III]	1908.7	5903.0	$2.101 \pm 0.005$	
IVS B0754–155	07 56 50.6989	–15 42 05.436	GS	C III]	1908.7	4618.2		
				C II]	2326.9	[5631.8]		
				Mg II	2799.9	6778.3	$1.4202 \pm 0.0007$	
IVS B0802–170	08 04 33.7013	–17 12 04.200	NTT	C III]	1908.7	3893.6		
				Mg II	2799.9	5727.0	$1.0427 \pm 0.0028$	
IVS B0810–180	08 12 28.5159	–18 10 42.813	GS	Ly $\alpha$	1215.7	4830.5		
				N V	1240.1	[4927.3]		
				C IV	1549.5	6154.3	$2.9726 \pm 0.0009$	*
IVS B0828–064	08 30 49.7439	–06 36 19.988	NTT	C IV	1549.5	4236.8		
				C III]	1908.7	5200.9	$1.730 \pm 0.005$	*
IVS B0828–222	08 31 09.1490	–22 28 26.804	NTT	C IV	1549.5	4031.3		
				C III]	1908.7	4958.6		
				Mg II	2799.9	7274.2	$1.5992 \pm 0.0012$	
IVS B0834–729	08 33 43.1410	–73 05 26.204	NTT	Si IV	1398.3	[4188.8]		
				C IV	1549.5	4630.8		
				C III]	1908.7	5707.0		
				Mg II	2799.9	[8389.8]	$1.9893 \pm 0.0007$	
IVS B0844–557	08 45 49.6795	–55 55 26.744	NTT	Mg II	2799.9	4026.5		

Table 1—Continued

Source	RA (J2000) <sup>a</sup>	Dec (J2000) <sup>a</sup>	Telescope <sup>b</sup>	Line	Rest $\lambda$	Obs $\lambda^c$	$\bar{z}$	Note <sup>d</sup>
				H $\gamma$	4340.5	[6246.6]		
				[O III]	4363.2	[6253.8]		
				H $\beta$	4861.3	6986.6		
				[O III]	4958.9	7105.9		
				[O III]	5006.8	7174.3	$0.4329 \pm 0.0001$	*
IVS B0859–068	09 01 44.2393	–07 02 16.067	NTT	Si IV	1398.3	[3852.0]		
				C IV	1549.5	4244.5		
				C III]	1908.7	5224.3		
				Mg II	2799.9	[7705.7]	$1.7382 \pm 0.0011$	
IVS B0909–745	09 09 20.9450	–74 45 08.148	NTT	C III]	1908.7	4268.1		
				Mg II	2799.9	6268.9	$1.2376 \pm 0.0014$	
IVS B0924–819	09 21 42.6981	–82 09 36.219	NTT	C III]	1908.7	[4363.4]		
				Mg II	2799.9	6413.4	$1.291 \pm 0.002$	S
IVS B0930–200	09 32 19.5864	–20 16 37.206	NTT	C III]	1908.7	4268.4		
				Mg II	2799.9	6260.1	$1.2361 \pm 0.0003$	
IVS B0948–860	09 41 55.6159	–86 15 01.817	GS	Ly $\alpha$	1215.7	5708.5		
				C IV	1549.5	7281.2	$3.6974 \pm 0.0017$	*
IVS B0950–246	09 52 31.6543	–24 53 50.885	NTT	Ly $\alpha$	1215.7	4410.0		
				Si IV	1398.3	[5084.7]		
				C IV	1549.5	5612.3		
				C III]	1908.7	[6959.4]	$2.6248 \pm 0.0028$	
IVS B0951+488	09 55 05.0011	+48 38 19.042	GN	[O II]	3726.8	5718.2		
				H $\beta$	4861.3	7455.6		
				[O III]	5006.8	7684.5	$0.5343 \pm 0.0003$	
IVS B0952–185	09 55 14.6807	–18 45 31.866	NTT	Ly $\alpha$	1215.7	[4779.7]		
				N V	1240.1	[4904.7]		
				Si IV	1398.3	5484.0		
				C IV	1549.5	6056.2		
				C III]	1908.7	7464.1	$2.9137 \pm 0.0042$	*
IVS B0956–409	09 58 38.2960	–41 10 33.176	NTT	Ly $\alpha$	1215.7	[4827.6]		
				N V	1240.1	[4902.2]		

Table 1—Continued

Source	RA (J2000) <sup>a</sup>	Dec (J2000) <sup>a</sup>	Telescope <sup>b</sup>	Line	Rest $\lambda$	Obs $\lambda^c$	$\bar{z}$	Note <sup>d</sup>
				Si iv	1398.3	[5544.5]		
				C iv	1549.5	6096.4		
				C iii]	1908.7	[7548.6]	$2.934 \pm 0.002$	S *
IVS B1004–125	10 07 15.2277	–12 47 45.995	GS	Si iv	1398.3	4369.8		
				C iv	1549.5	4833.0		
				C iii]	1908.7	5964.4	$2.1230 \pm 0.0020$	* $z = 0.24$ [S]
IVS B1005–739	10 06 04.1454	–74 09 44.087	NTT	Ly $\alpha$	1215.7	3959.0		
				Si iv	1398.3	4533.3		
				C iv	1549.5	5028.5		
				C iii]	1908.7	6153.4	$2.242 \pm 0.007$	
IVS B1010–374	10 12 24.0748	–37 40 05.899	NTT	Mg ii	2799.9	4196.4		
				[O ii]	3726.8	[5562.4]		
				[Ne III]	3869.1	5793.8		
				H $\gamma$	4340.5	6503.4		
				[O iii]	4363.2	6539.5		
				H $\beta$	4861.3	7292.8		
				[O iii]	4958.9	[7420.3]		
				[O iii]	5006.8	7506.9	$0.4991 \pm 0.0003$	
IVS B1013–196	10 15 52.2525	–19 52 26.567	GS	Mg ii	2799.9	5827.5		
				[Ne v]	3425.5	[7127.5]	$1.081 \pm 0.001$	S $z = 1.0865$ [6dF]
IVS B1020+270	10 20 11.1028	+26 49 41.724	NOT	Si iv	1398.3	5294.9		
				C iv	1549.5	5876.7	$2.7900 \pm 0.0030$	
IVS B1023–049	10 25 45.4229	–05 09 54.132	NTT	C iii]	1908.7	4050.3		
				Mg ii	2799.9	5961.1	$1.1255 \pm 0.0035$	
IVS B1034–058	10 36 47.5730	–06 05 41.184	NTT	C iii]	1908.7	3915.8		
				Mg ii	2799.9	5736.7	$1.0502 \pm 0.0013$	
IVS B1035+046	10 37 39.3395	+04 24 01.745	NOT	C iv	1549.5	5154.0		
				C iii]	1908.7	6316.8	$2.318 \pm 0.008$	
IVS B1039–474	10 41 44.6497	–47 40 00.064	GS	Ly $\alpha$	1215.7	4324.1		
				N v	1240.1	[4421.6]		
				Si iv	1398.3	4981.2		

Table 1—Continued

Source	RA (J2000) <sup>a</sup>	Dec (J2000) <sup>a</sup>	Telescope <sup>b</sup>	Line	Rest $\lambda$	Obs $\lambda^c$	$\bar{z}$	Note <sup>d</sup>
				C IV	1549.5	5507.2		
				C III]	1908.7	6792.5	$2.5580 \pm 0.0017$	*
IVS B1055–028	10 58 11.0106	–03 09 27.254	GN	[O II]	3726.8	6367.3		
				H $\gamma$	4340.5	[7419.4]		
				[O III]	4363.2	[7451.9]		
				H $\beta$	4861.3	[8306.2]		
				[O III]	4958.9	8468.6		
				[O III]	5006.8	8553.0	$0.7082 \pm 0.0002$	
IVS B1102–392	11 05 11.0815	–39 28 42.138	NTT	C IV	1549.5	4042.6		
				C III]	1908.7	4981.9		
				Mg II	2799.9	7320.5	$1.6112 \pm 0.0017$	
IVS B1104+525	11 07 25.8277	+52 19 31.636	NOT	Mg II	2799.9	5443.8	$0.944 \pm 0.002$	S
IVS B1115–306	11 18 20.6102	–30 54 58.520	GS	Si IV	1398.3	[4701.3]		
				C IV	1549.5	5194.6		
				C III]	1908.7	6400.0	$2.3528 \pm 0.0004$	
IVS B1119–044	11 21 43.1144	–04 42 36.149	NTT	C IV	1549.5	4230.9		
				C III]	1908.7	5211.4		
				Mg II	2799.9	[7660.0]	$1.7304 \pm 0.0002$	
IVS B1121–147	11 24 02.5656	–15 01 58.948	NTT	Ly $\alpha$	1215.7	[4345.9]		
				N V	1240.1	[4422.3]		
				Si IV	1398.3	[4990.1]		
				C IV	1549.5	5517.5		
				C III]	1908.7	6796.0	$2.5607 \pm 0.0003$	
IVS B1121+661	11 24 24.6667	+65 55 01.380	GN	[O II]	3726.8	5731.3		
				[O III]	5006.8	7699.9	$0.5379 \pm 0.0001$	
IVS B1127–443	11 29 31.7220	–44 35 49.937	GS	[O II]	3726.8	4906.7	$0.317 \pm 0.001$	S *
IVS B1129–161	11 31 36.7478	–16 28 33.439	NTT	Mg II	2799.9	4999.7	0.786 :	S
IVS B1131–088	11 33 35.9928	–09 05 23.401	NTT	C III]	1908.7	3804.5		
				Mg II	2799.9	5574.2	$0.9920 \pm 0.0012$	



Table 1—Continued

Source	RA (J2000) <sup>a</sup>	Dec (J2000) <sup>a</sup>	Telescope <sup>b</sup>	Line	Rest $\lambda$	Obs $\lambda^c$	$\bar{z}$	Note <sup>d</sup>
IVS B1143–696	11 45 53.6241	–69 54 01.797	GS	H $\epsilon$	3970.1	4939.2	0.2434 $\pm$ 0.0003	*
				H $\delta$	4101.7	5102.7		
				H $\gamma$	4340.5	5399.8		
				H $\beta$	4861.3	6043.9		
				[O III]	4958.9	6160.7		
				[O III]	5006.8	6222.2		
IVS B1152+462	11 55 11.0092	+45 55 39.624	GN	[O II]	3726.8	6387.0	0.7141 $\pm$ 0.0002	
				[Ne III]	3868.7	[6626.9]		
				[O III]	4958.9	8500.2		
				[O III]	5006.8	8583.2		
IVS B1223+452	12 25 54.619	+44 56 23.01	NOT	[O II]	3726.8	6230.0	0.6716 $\pm$ 0.0001	
				[Ne III]	3868.7	6467.2		
IVS B1241+410	12 43 55.7815	+40 43 58.451	NOT	C III]	1908.7	4806.4	1.5181 $\pm$ 0.0002	
				Mg II	2799.9	7050.3		
IVS B1338+362	13 40 36.0099	+36 00 26.737	NOT	[O II]	3726.8	6564.5	0.7632 $\pm$ 0.0016	
				Ca K	3937.8	6956.1		
				Ca H	3969.6	6993.5		
IVS B1446–111	14 48 51.1600	–11 22 15.737	GS	Ly $\alpha$	1215.7	4416.3	2.6326 $\pm$ 0.0004	
				N V	1240.1	[4506.0]		
				Si IV	1398.3	[5080.7]		
				C IV	1549.5	5628.4		
				He II	1640.4	5960.1		
				C III]	1908.7	6932.0		
IVS B1533+200	15 35 16.560	+19 54 51.30	NOT	Ly $\alpha$	1215.7	5582.7	3.5899 $\pm$ 0.0023	
				N V	1240.1	[5692.8]		
				C IV	1549.5	7108.4		
IVS B1607+563	16 08 20.7501	+56 13 56.375	NOT	Si IV	1398.3	[5723.5]	3.0840 $\pm$ 0.0010	
				C IV	1549.5	6329.8		
				He II	1640.4	6697.8		
IVS B1630+505	16 31 31.6980	+50 28 22.493	NOT	C IV	1549.5	5179.4	2.348 $\pm$ 0.005	
				He II	1640.4	[5497.3]		
				C III]	1908.7	6400.0		

Table 1—Continued

Source	RA (J2000) <sup>a</sup>	Dec (J2000) <sup>a</sup>	Telescope <sup>b</sup>	Line	Rest $\lambda$	Obs $\lambda^c$	$\bar{z}$	Note <sup>d</sup>
IVS B1641–179	16 44 35.7468	–18 04 32.459	GS	Mg II	2799.9	5619.4	$1.007 \pm 0.001$	S
IVS B1722+562	17 22 58.0084	+56 11 22.320	NOT	Ly $\alpha$	1215.7	3976.2	$2.269 \pm 0.005$	*
				C IV	1549.5	5077.9		
				C III]	1908.7	6222.9		
IVS B1744–629	17 49 25.7102	–62 58 18.950	GS	C III]	1908.7	[4228.8]	$1.215 \pm 0.001$	S
				Mg II	2799.9	6202.1		
IVS B2107–016	21 10 22.6190	–01 26 58.242	GN	Mg II	2799.9	5331.3	$0.9043 \pm 0.0002$	
				[Ne V]	3425.5	6525.0		
				[O II]	3726.8	7095.6		
				[Ne III]	3868.7	7366.9		
				H $\gamma$	4340.5	[8263.8]		
				[O III]	4363.2	[8308.3]		
IVS B2112–556	21 16 29.8161	–55 27 20.444	GS	C IV	1549.5	4215.5	$1.7216 \pm 0.0011$	
				C III]	1908.7	5196.8		
IVS B2142–765	21 47 53.1505	–76 21 29.221	GS	C IV	1549.5	4464.5	$1.8841 \pm 0.0029$	
				C III]	1908.7	5510.3		
IVS B2144–065	21 47 21.8896	–06 20 25.342	GN/BTA	Mg II	2799.9	5056.1	$0.8058 \pm 0.0001$	
				[Ne V]	3425.5	6186.8		
				[O II]	3726.8	6729.5		
				[Ne III]	3868.7	6986.2		
				[Ne III]	3967.8	7166.1		
				H $\delta$	4101.7	7406.9		
				H $\gamma$	4340.5	7836.8		
				[O III]	4363.2	7878.0		
IVS B2201–778	22 06 44.4595	–77 35 23.761	GS	Mg II	2799.9	5544.1	$0.980 \pm 0.001$	S
IVS B2202+716	22 03 30.4676	+71 51 08.530	GN	Mg II	2799.9	7097.4	$1.535 \pm 0.001$	S
IVS B2235–556	22 39 06.0344	–55 25 59.410	GS	C IV	1549.5	[4591.7]	$1.975 \pm 0.001$	S *
				C III]	1908.7	5678.2		
IVS B2251–597	22 54 56.8282	–59 26 00.683	GS	C IV	1549.5	4523.4		

Table 1—Continued

Source	RA (J2000) <sup>a</sup>	Dec (J2000) <sup>a</sup>	Telescope <sup>b</sup>	Line	Rest $\lambda$	Obs $\lambda^c$	$\bar{z}$	Note <sup>d</sup>
				C III]	1908.7	5569.5	$1.9186 \pm 0.0007$	
IVS B2253+227	22 56 10.6750	+23 01 45.175	GN	C III]	1908.7	5404.3		
				Mg II	2799.9	7925.2	$1.8310 \pm 0.0005$	
IVS B2253–658	22 56 24.8717	–65 33 25.648	GS	[Ne III]	3868.7	4826.9		
				H $\epsilon$	3970.1	[4953.2]		
				H $\delta$	4101.7	[5125.5]		
				H $\gamma$	4340.5	[5415.1]		
				[O III]	4363.2	[5442.1]		
				H $\beta$	4861.3	6066.5		
				[O III]	4958.9	6186.7		
				[O III]	5006.8	6246.9	$0.2477 \pm 0.0001$	
IVS B2300–307	23 03 05.8207	–30 30 11.473	NTT	C III]	1908.7	3887.4		
				Mg II	2799.9	5714.3	$1.0388 \pm 0.0021$	
IVS B2303+083	23 06 01.2714	+08 37 15.391	GN	Mg II	2799.9	6456.8		
				[Ne V]	3425.5	7890.3		
				[O II]	3726.8	8598.7	$1.3056 \pm 0.0011$	
IVS B2309–663	23 12 58.8400	–66 07 31.735	GS	He II	1640.4	[4326.3]		
				C III]	1908.7	5035.1		
				[Ne IV]	2423.8	[6393.6]	$1.638 \pm 0.001$	S
IVS B2325–408	23 28 19.2648	–40 35 09.846	GS	C IV	1549.5	4598.8		
				C III]	1908.7	5680.3	$1.972 \pm 0.004$	
IVS B2334–525	23 37 23.1667	–52 16 20.103	GS	C II]	2326.9	[5016.6]		
				Mg II	2799.9	6080.1	$1.172 \pm 0.002$	S *
IVS B2341+295	23 44 22.5524	+29 52 20.700	GN	Mg II	2799.9	5454.4		
				[Ne V]	3425.5	[6657.1]		
				[O II]	3726.8	7264.1		
				[Ne III]	3868.7	7538.5	$0.9486 \pm 0.0003$	*
IVS B2355+042	23 58 28.8469	+04 30 24.835	GN	C IV	1549.5	5109.4		
				C III]	1908.7	6285.7	$2.2953 \pm 0.0021$	$z = 2.294$ [A09]

<sup>a</sup>ICRF2 radio position

<sup>b</sup>Telescope abbreviations: BTA = Big Azimuthal Telescope, GS = Gemini North, NOT = Nordic Optical Telescope, NTT = ESO New Technology Telescope

<sup>c</sup>Square brackets indicate the line was not used for redshift determination

<sup>d</sup>“S” denotes a single-line redshift; \* indicates a note in Section 3.2. Previously determined redshifts are from: [A09] Afanas’ev et al. (2009); [S12] Shaw et al. (2012); [S] Simbad database; [6dF] 6dF survey, Jones et al. (2009)

Table 2. Probable BL Lac objects

Source	RA (J2000) <sup>a</sup>	Dec (J2000) <sup>a</sup>	Telescope
IVS B0026–710	00 28 41.5626	–70 45 15.926	GS
IVS B0313–171	03 15 27.6783	–16 56 29.711	NTT
IVS B0608–187	06 10 17.8861	–18 47 40.090	GS
IVS B0633–263	06 35 20.9090	–26 20 39.866	NTT
IVS B0700–661	07 00 31.2531	–66 10 45.232	NTT
IVS B0729–826	07 23 39.4063	–82 47 41.089	NTT
IVS B0744–158	07 46 18.2360	–15 55 34.745	NTT
IVS B0752–116	07 54 26.4564	–11 47 16.948	GS
IVS B0804–055	08 07 09.6175	–05 41 13.914	NTT
IVS B0815–094	08 17 49.7495	–09 33 30.528	GS
IVS B1123–356	11 25 31.4818	–35 57 03.352	NTT
IVS B1424–328	14 27 41.3610	–33 05 31.505	GS
IVS B1922–224	19 25 39.7901	–22 19 35.112	GS
IVS B1942–313	19 45 59.3693	–31 11 38.356	GS
IVS B1951–115	19 54 41.1557	–11 23 22.641	GS
IVS B2022–289	20 25 53.6128	–28 45 48.697	GS
IVS B2036–109	20 39 00.7104	–10 46 41.863	GS
IVS B2104–668	21 08 51.8207	–66 37 22.744	GS
IVS B2240–064	22 43 08.7606	–06 09 02.567	GN

<sup>a</sup>ICRF2 radio position

Table 3. Objects with low signal-to-noise spectra

Source	RA (J2000) <sup>a</sup>	Dec (J2000) <sup>a</sup>	Telescope
IVS B0205–242	02 07 33.3992	–24 02 02.210	NTT
IVS B0227–542	02 29 12.7856	–54 03 24.036	NTT
IVS B0244–050	02 46 49.1315	–04 51 10.933	NTT
IVS B0253–754	02 53 10.8816	–75 13 16.686	GS
IVS B0334–546	03 35 53.9248	–54 30 25.114	NTT
IVS B0458+138	05 01 45.2708	+13 56 07.220	NTT
IVS B0516–621	05 16 44.9261	–62 07 05.389	NTT
IVS B0600+219	06 03 51.5570	+21 59 37.698	GN
IVS B0628–627	06 28 57.4877	–62 48 44.744	NTT
IVS B0705–649	07 05 26.0526	–65 00 43.484	NTT
IVS B0718–523	07 19 14.2919	–52 28 32.506	NTT
IVS B0821–094	08 23 52.0233	–09 39 25.907	NTT
IVS B0905–202	09 07 54.0404	–20 26 49.475	GS
IVS B0939–077	09 42 21.4614	–07 59 53.204	GS
IVS B1118+073	11 20 38.4438	+07 04 47.174	NTT
IVS B1134–739	11 36 09.6597	–74 15 45.274	NTT
IVS B1821–525	18 25 13.8097	–52 30 58.281	GS
IVS B2020–015	20 23 32.8163	–01 23 42.153	GS

<sup>a</sup>ICRF2 radio position



Table 4. SDSS magnitudes and redshifts for five color-selected NVSS radio sources

Source	RA (J2000) <sup>a</sup>	Dec (J2000) <sup>a</sup>	$g$	$r$	Telescope <sup>b</sup>	Line	Rest $\lambda$	Obs $\lambda^c$	$z^d$
NVSS J101335+281118	10 13 35.49	+28 11 18.3	25.76	22.03	NOT	$\text{Ly } \alpha$	1215.7	6990	4.75:
						$\text{Ly } \beta$	1025.7	5897	
NVSS J125944+240707	12 59 44.59	+24 07 07.9	22.94	21.82	NOT	$\text{Mg II}$	2799.9	5895.5	$1.138 \pm 0.001$
NVSS J145459+110928	14 54 59.36	+11 09 28.5	26.09	22.67	NOT	$\text{Ly } \alpha$	1215.7	7208	4.93:
NVSS J162830+115403	16 28 30.55	+11 54 03.5	25.27	22.25	NOT	$\text{Ly } \alpha$	1215.7	6650	4.47:
NVSS J163400+640821	16 34 00.47	+64 08 21.6	24.67 <sup>e</sup>	19.57 <sup>e</sup>	NOT	$\text{Ly } \alpha$	1215.7	[5628.4]	$3.619 \pm 0.001$
						O I/Si II	1303.3	[6039.0]	
						Si IV	1398.3	[6458.1]	
						C IV	1549.5	7157.7	

<sup>a</sup>NVSS radio position

<sup>b</sup>Nordic Optical Telescope

<sup>c</sup>Square brackets indicate the line was not used for redshift determination

<sup>d</sup>Colon indicates approximate redshift based on  $\text{Ly } \alpha$  alone

<sup>e</sup>Magnitudes are  $u$  and  $g$ , respectively, for this object

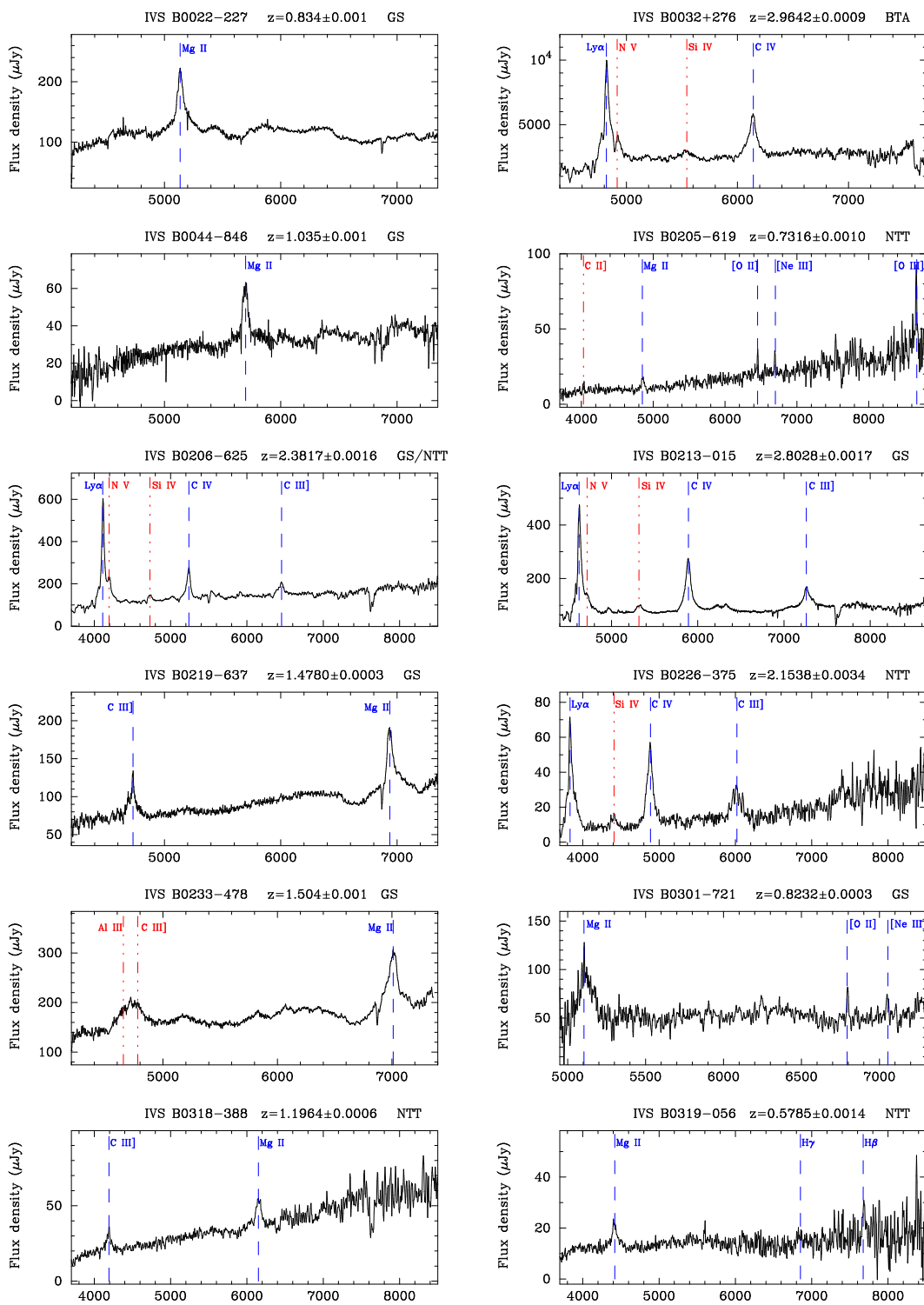


Fig. 1.— Optical spectra for 120 emission-line IVS targets. Dashed lines (blue) indicate emission lines used for redshift determination; dot-dashed lines (red) indicate lines detected at a lower signal-to-noise ratio or blended.

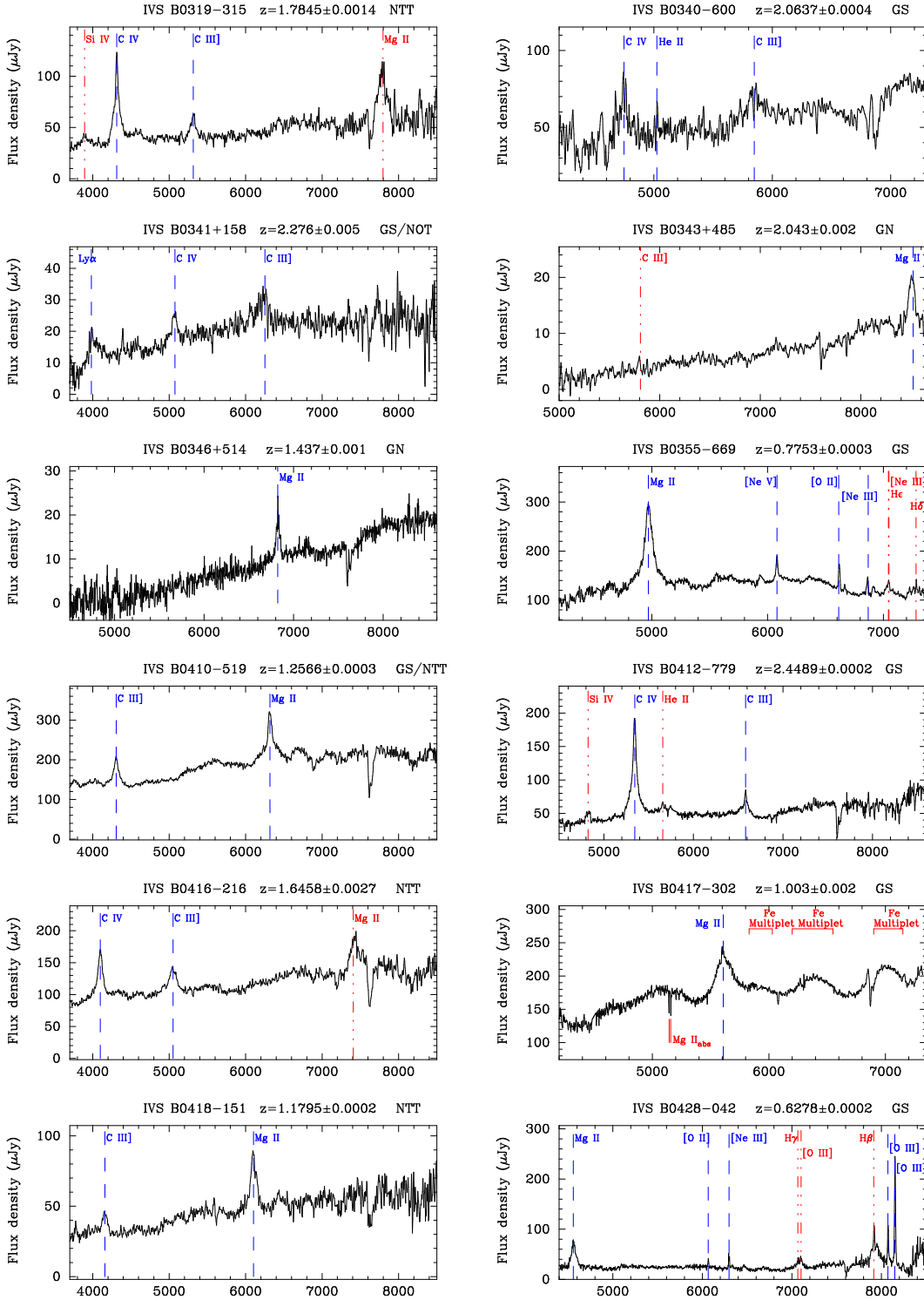


Fig. 1 (continued).—

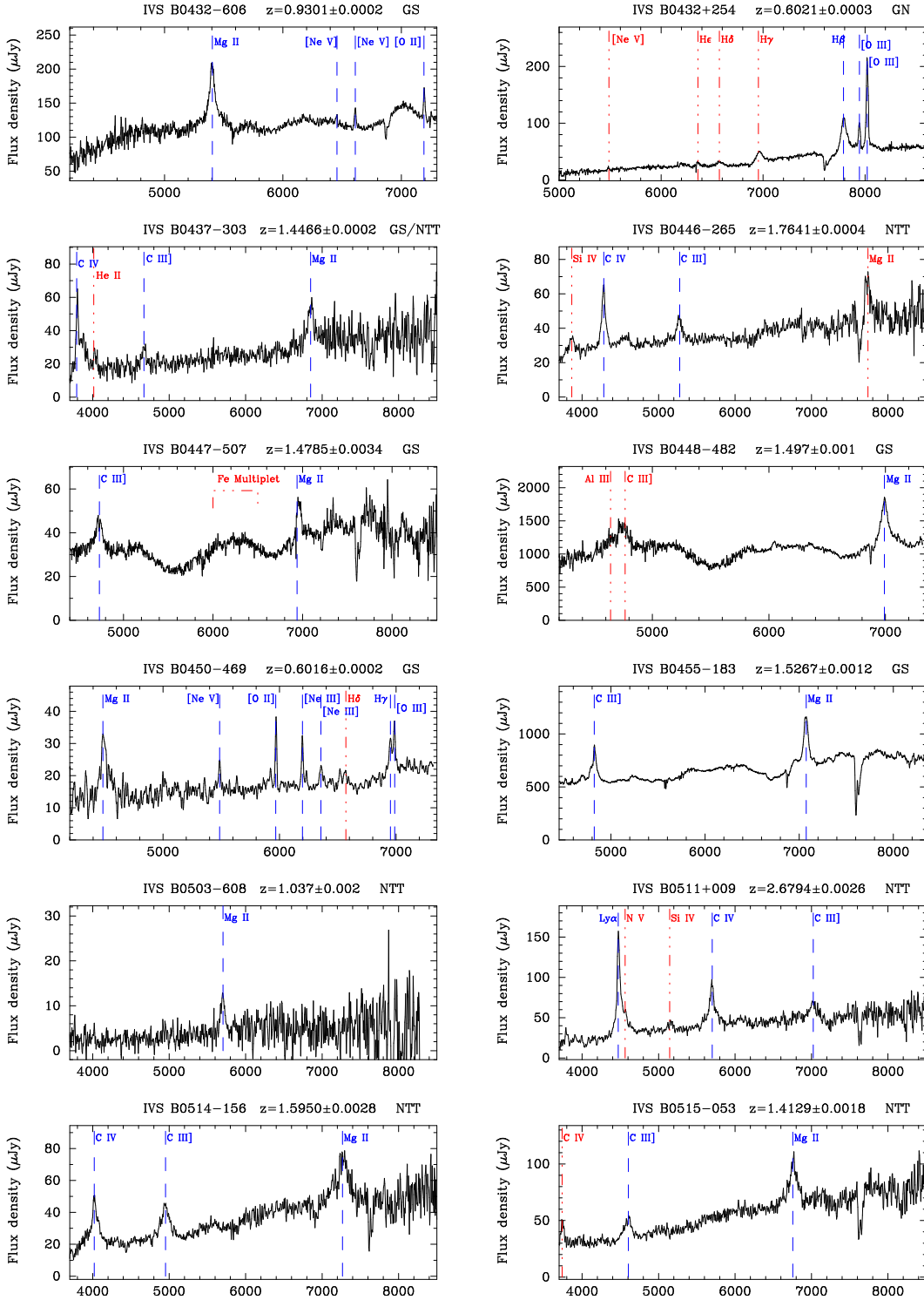


Fig. 1 (continued).—

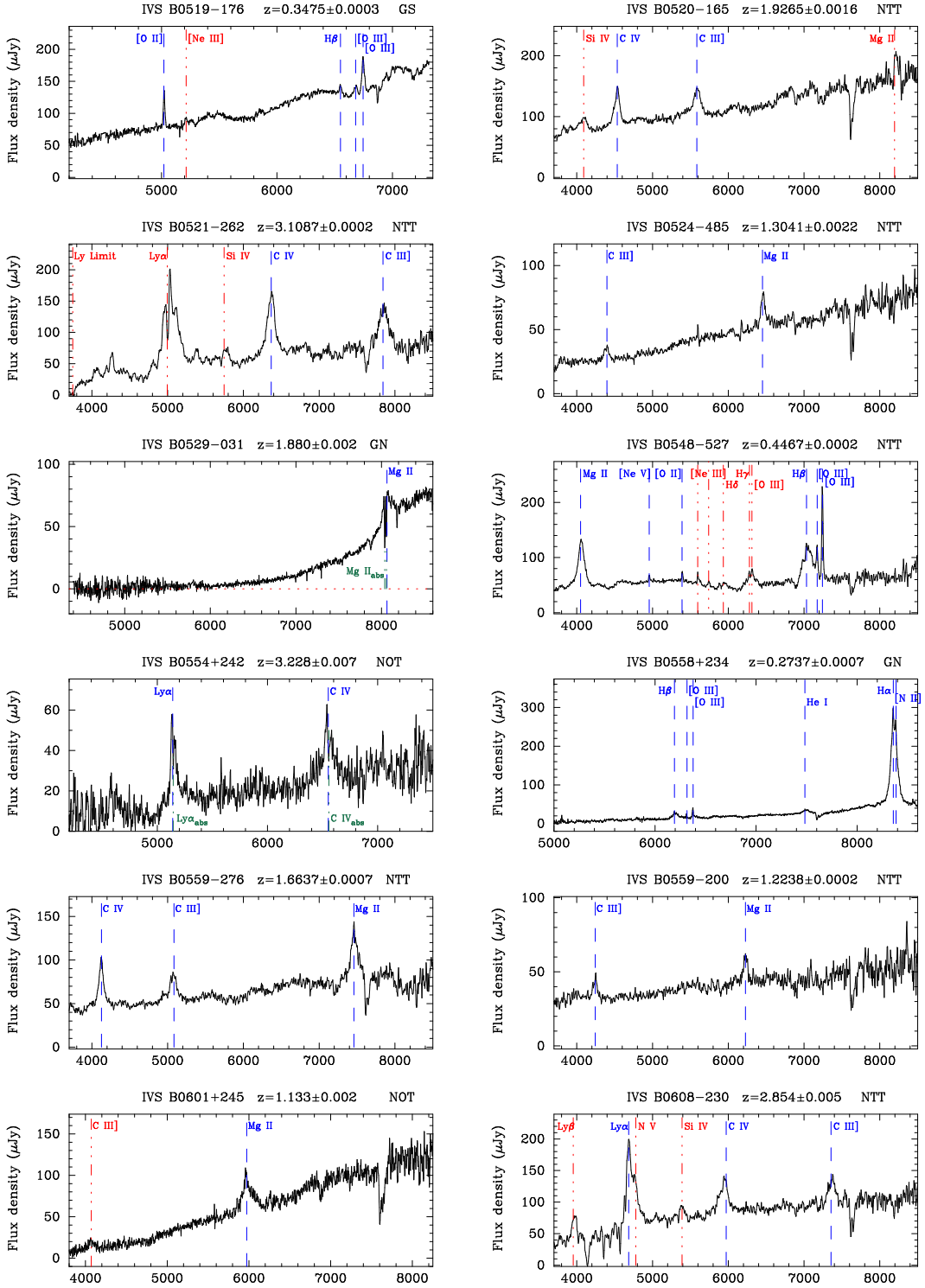


Fig. 1 (continued).—

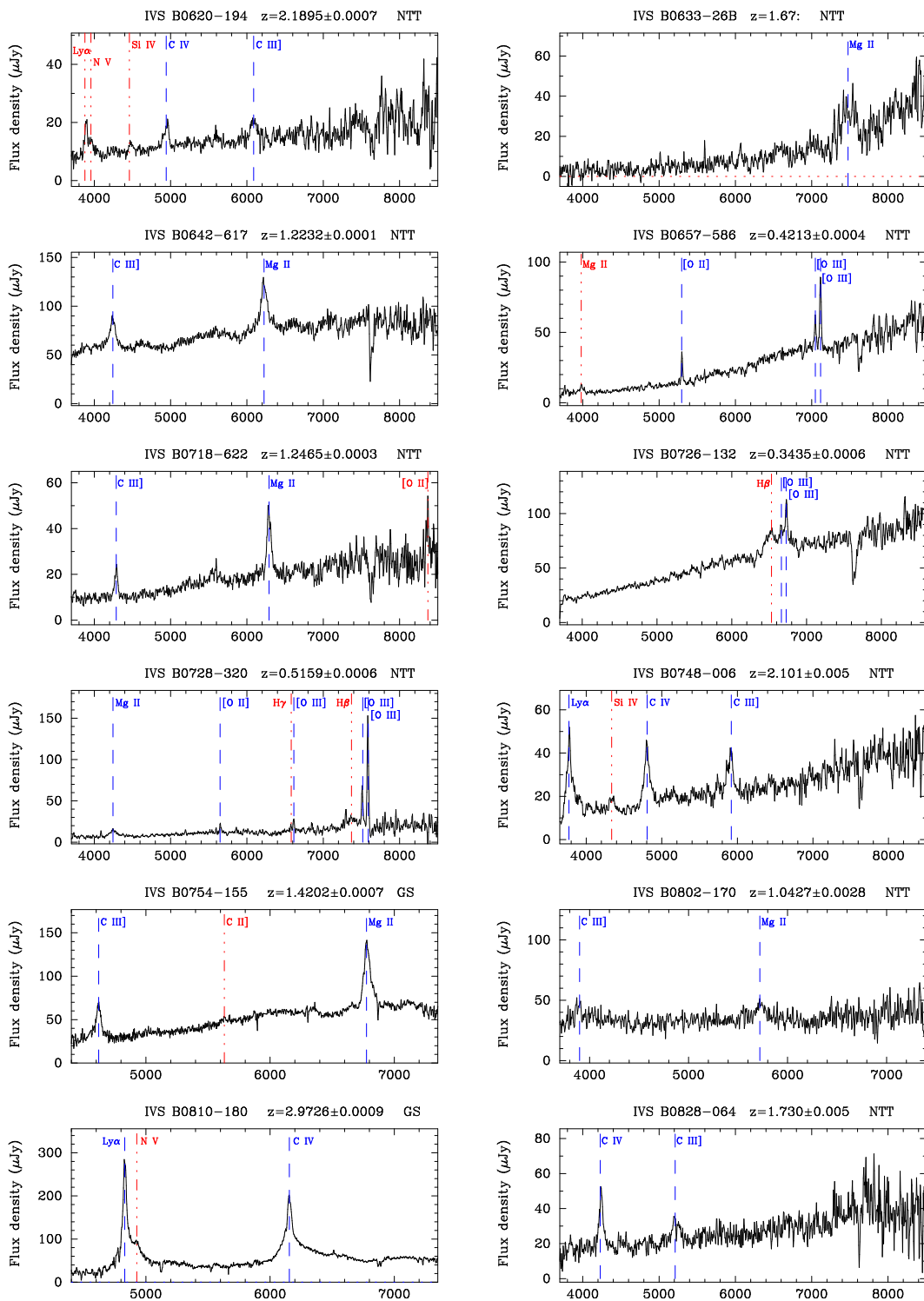


Fig. 1 (continued).—

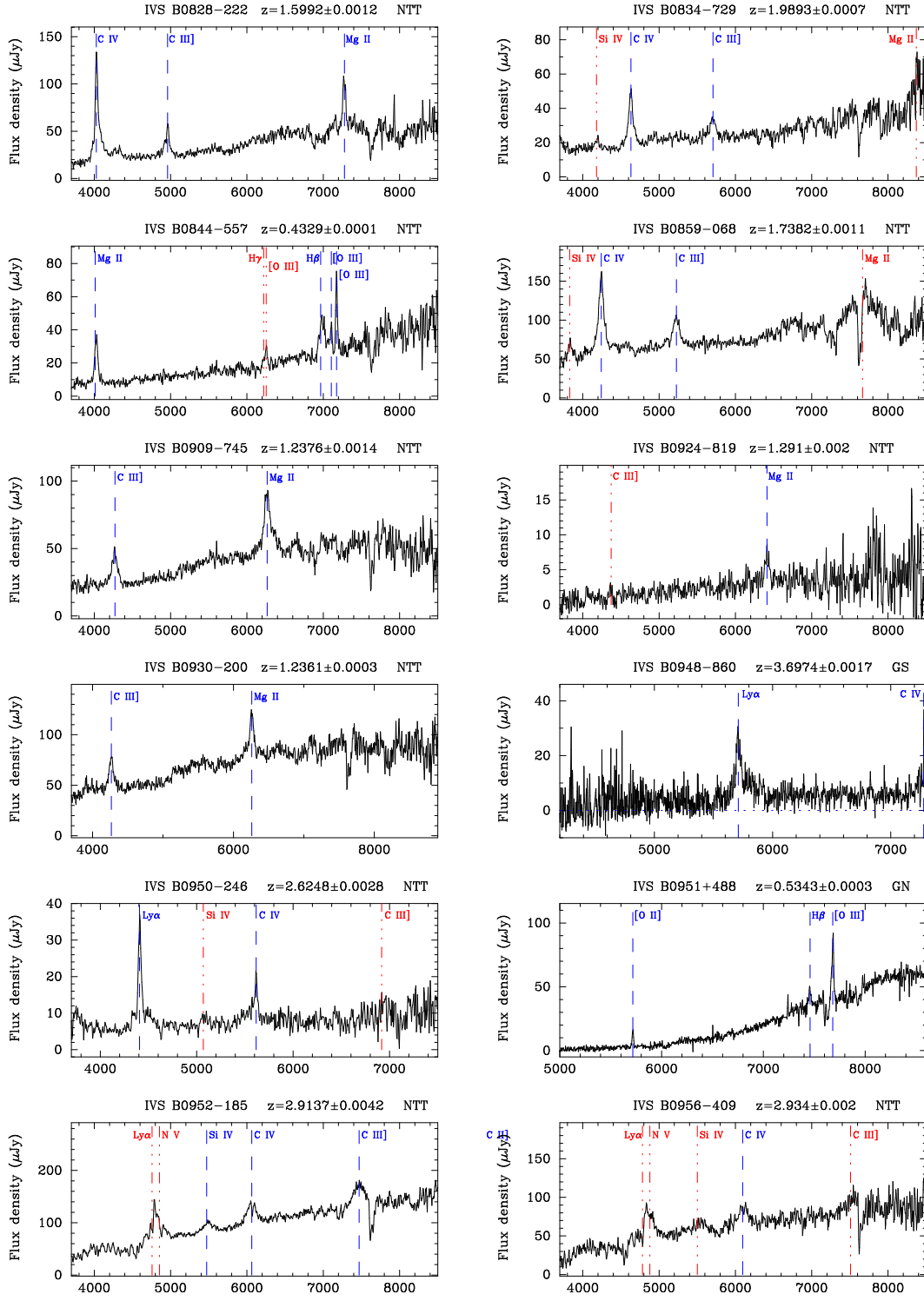


Fig. 1 (continued).—

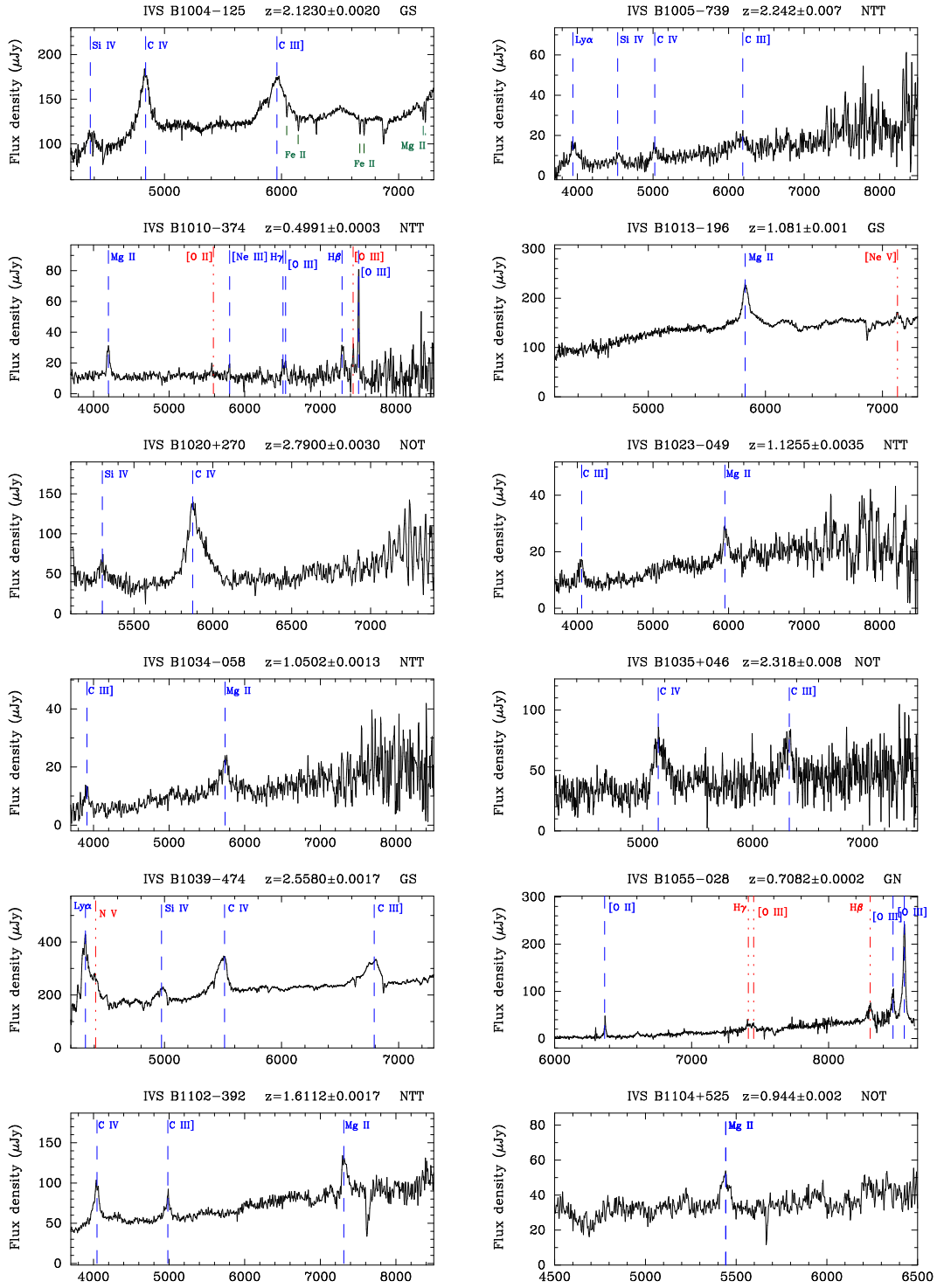


Fig. 1 (continued).—



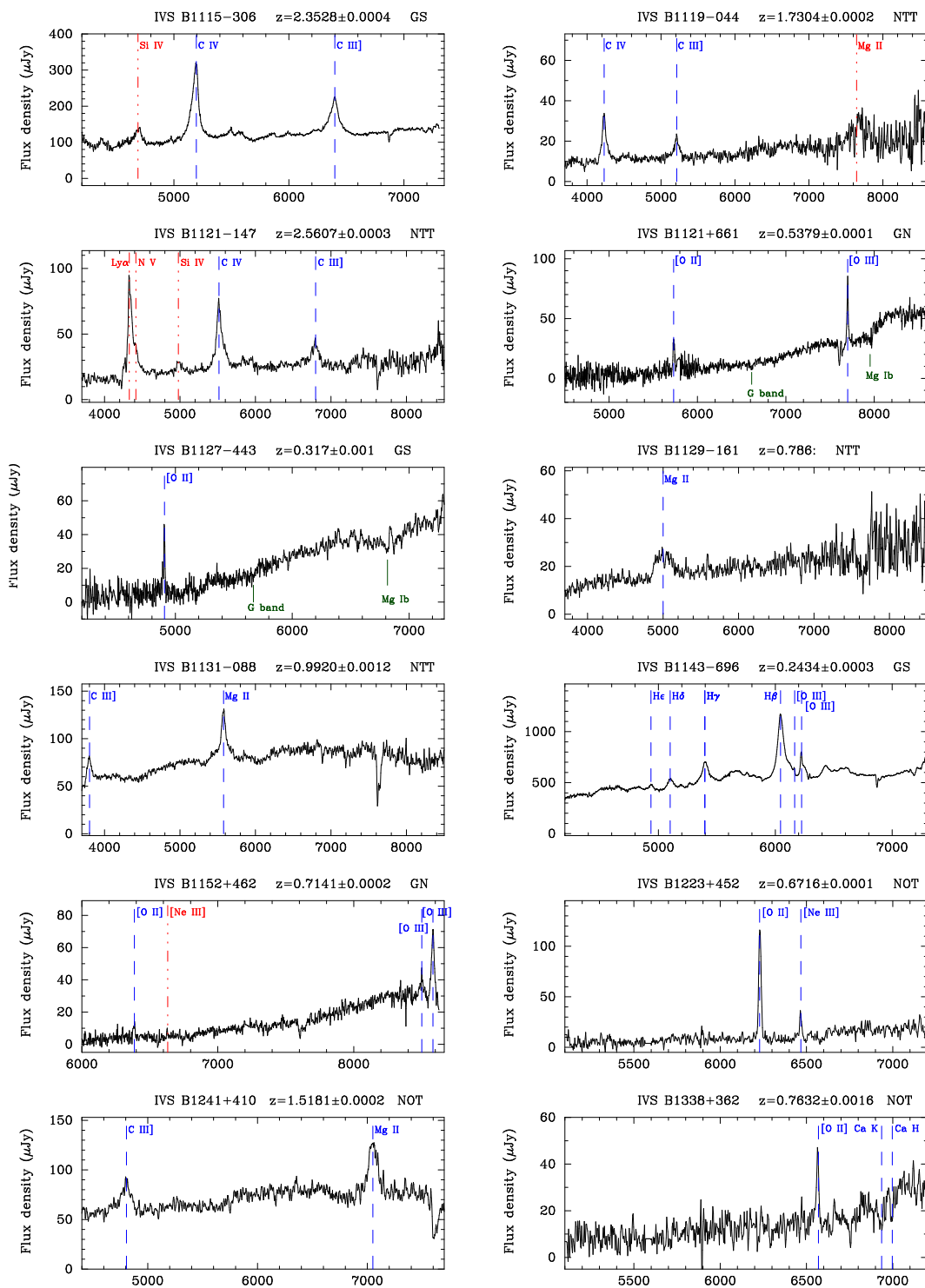


Fig. 1 (continued).—

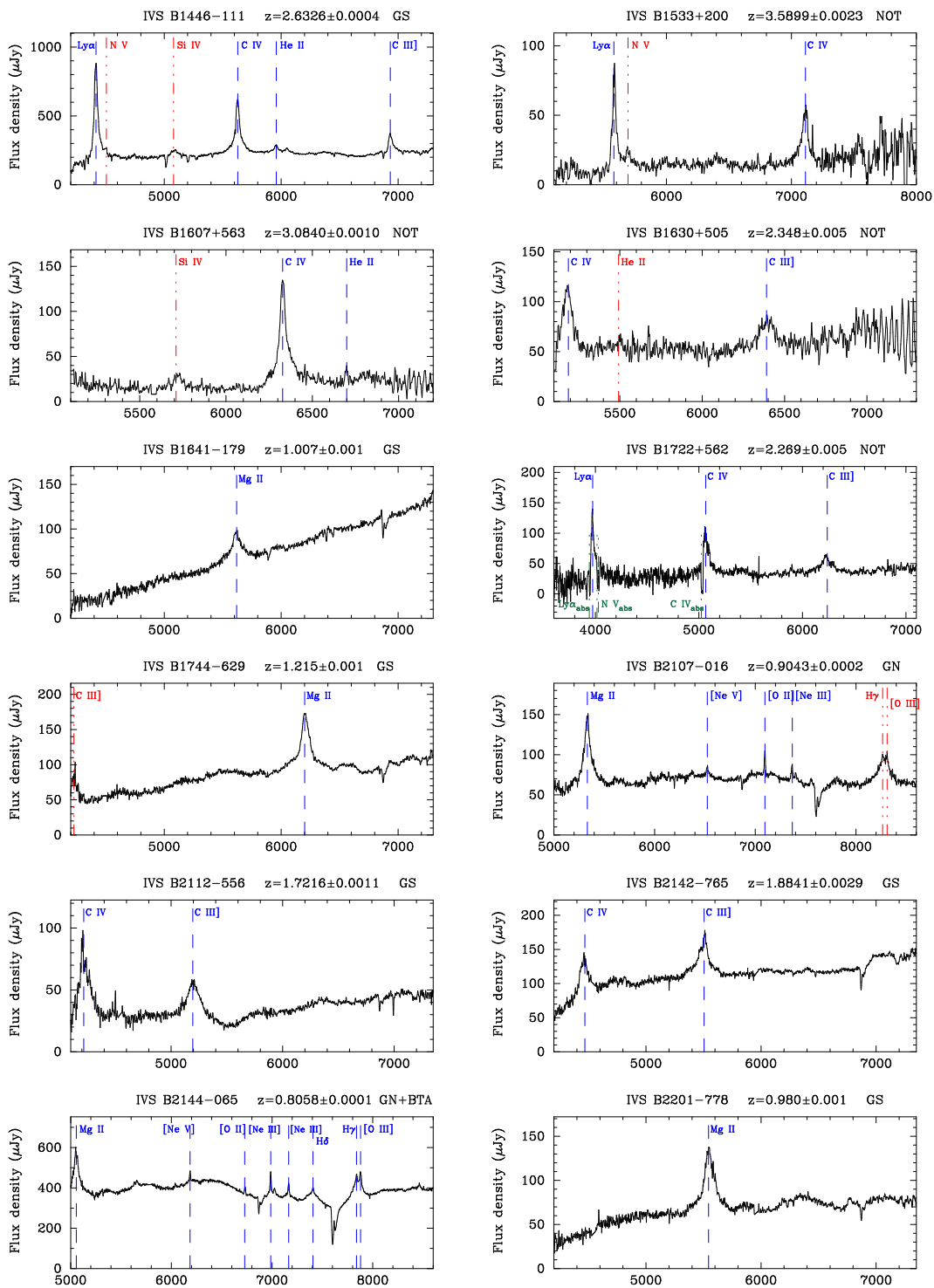


Fig. 1 (continued).—

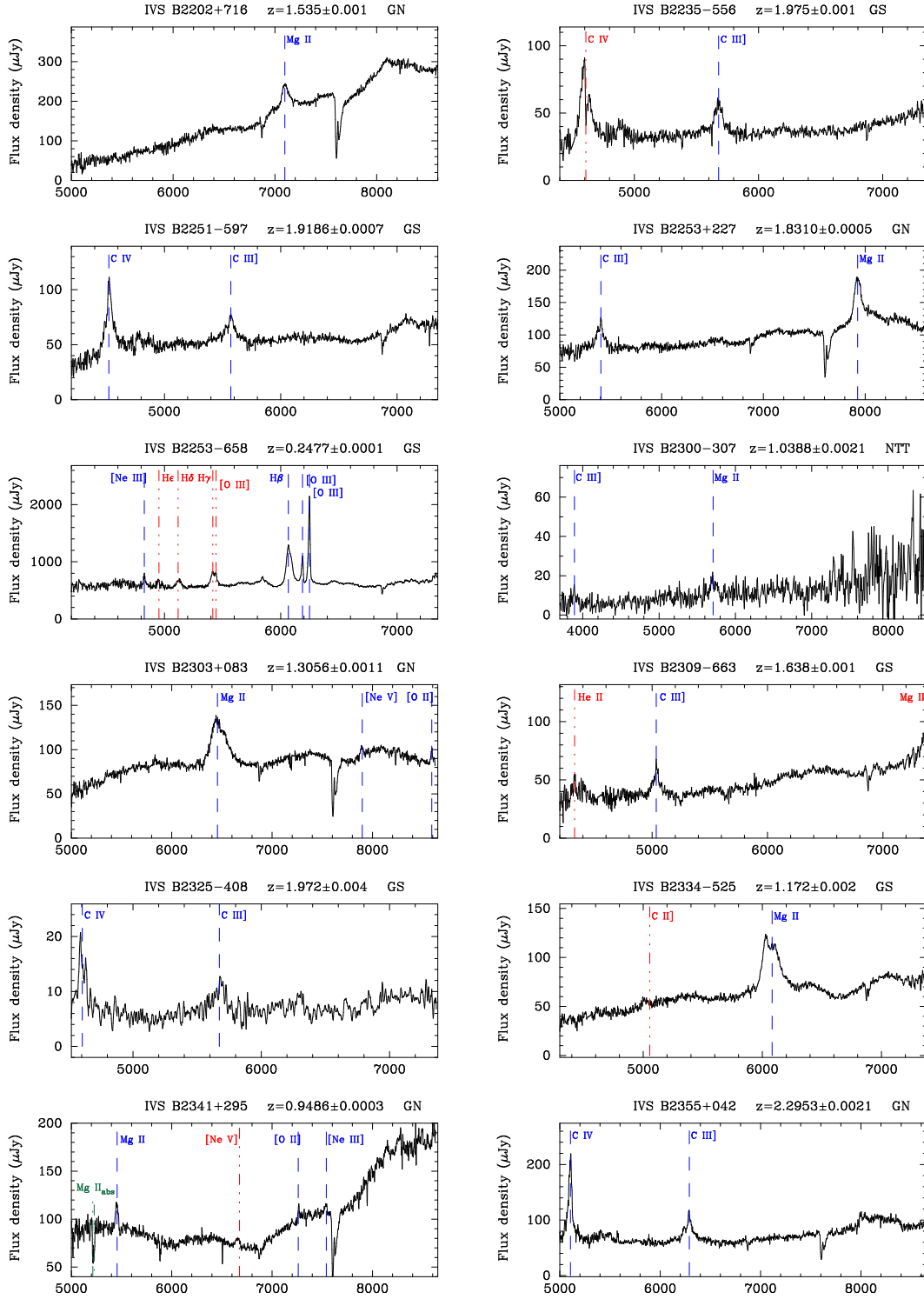


Fig. 1 (continued).—

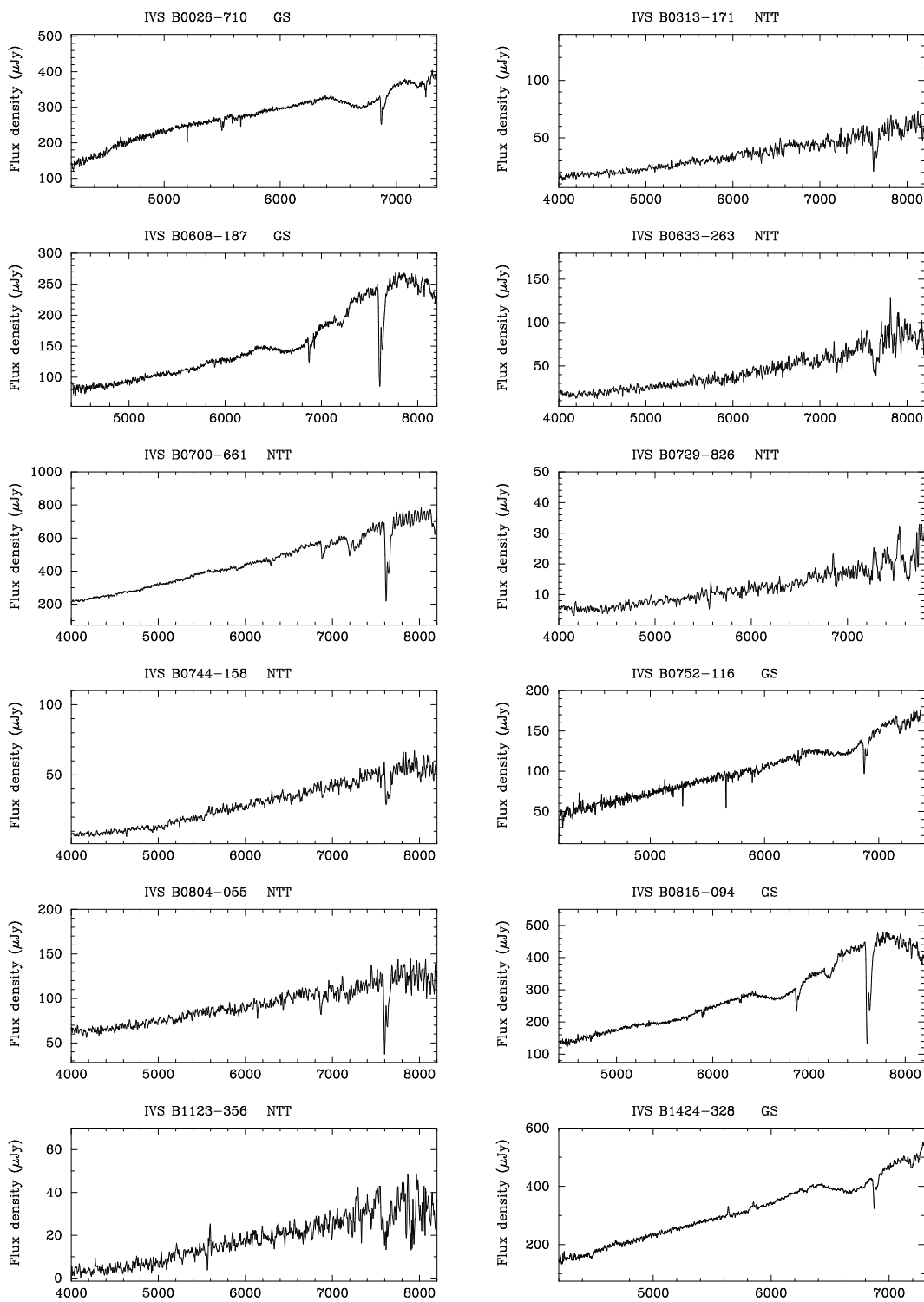


Fig. 2.— Spectra of 19 probable BL Lac objects from our observations, classified on the basis of their featureless spectra; see Table 2 for ICRF2 positions.

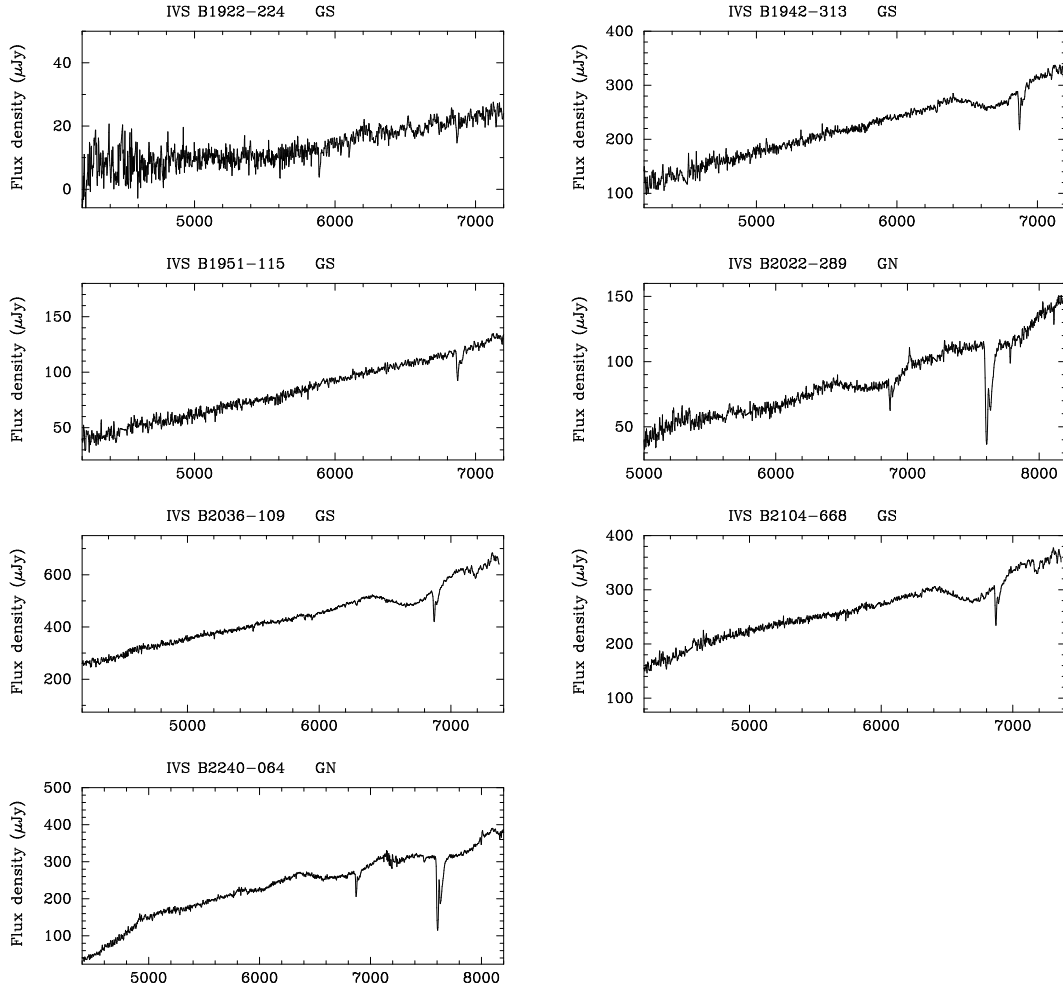


Fig. 2 (continued).—